Investigating Mitochondrial Choline Metabolism in Macrophages

Ciara Pember

Thesis submitted to the University of Ottawa
in partial Fulfillment of the requirements
for the degree of Master of Science in Biochemistry

Department of Biochemistry, Microbiology, and Immunology
Faculty of Medicine
University of Ottawa

Abstract

The essential nutrient choline is known to serve as a precursor for phospholipids and the neurotransmitter acetylcholine, and to feed into methylation pathways. The role and fate of choline in immune cells, however, is not yet fully elucidated. To act as a methyl group donor, choline must first undergo oxidation in mitochondria, a process which has long been thought to occur exclusively in the liver and kidney. The recent identification of choline transporters on the mitochondrial membrane has highlighted the possibility of mitochondrial choline oxidation in other cell types. Here, I show that choline transporters are present on the mitochondrial membrane of primary and immortalized mouse macrophages. The interaction of CTL2 with mitochondria is further augmented following pro-inflammatory polarization with the bacterial endotoxin lipopolysaccharide. I show that mitochondrial choline uptake occurs in macrophages using radiolabelled choline assays; however, it remains unclear whether this process is conducted through the identified transporters. Preliminary data suggest that mitochondrial choline oxidation to betaine was increased in LPS-stimulated macrophages, revealing a potential additional input into one-carbon metabolism in polarized macrophages. This project broadens the existing paradigm that choline oxidation occurs strictly in hepatic and renal tissue and suggests that choline oxidation may be a regulated process in macrophage polarization.

Acknowledgments

Thank you to my supervisor Dr. Morgan Fullerton. It has been a great privilege to be a part of the lab these past few years and I have immense gratitude for instilling in me the confidence to further my education in the world of immunometabolism here in Ottawa. It has been a pleasure to be a part of *the lab with heart*. I am also grateful for the support and advice of Dr. Erin Mulvihill and Dr. Mireille Khacho of my Thesis Advisory Committee.

Great thanks to my lab: to Tyler and Julia for their support, banter, and impromptu dance sessions. Conor for answering my quiet questions and a huge shoutout to Peyman who has taught me lots and put up with my initial disagreement towards much of it. Cheers to Lucia, Claire, Luke, Chantal, Matt, Alexanne, Mahrukh, Jeremy, and George for their encouragement and support. To Peter, Julianna, and Nadya for supporting crazy ideas. To Chloe and Sue, thank you for being inspirational women in STEM. Thank you to Chloe and Redaet, in their roles at the CBIA core, who were tremendously helpful in developing my microscopy technical skills and I am grateful for their patience and wisdom through the process.

What I have learned from this amazing group of people made every sideways Western worth the opportunity to do it.

Table of Contents

List of Figures

List of Tables

Abbreviations

AMPK	AMP-activated protein kinase
BADH	Betaine aldehyde dehydrogenase
BMDM	Bone marrow-derived macrophage
BHMT	Betaine-homocysteine S-methyltransferase
CDP	Cytidine 5'-diphosphocholine
CHDH	Choline dehydrogenase
CHT1	High affinity choline transporter
CTL	Choline transporter-like protein
DAG	Diacylglycerol
DAMP	Damage-associated molecular pattern
Drp1	Dynamin related protein 1
EM	Electron microscopy
Free	Free choline
GM-CSF	Growth factor macrophage colony stimulating factor
HC-3	Hemicholinium-3
IF	Immunofluorescence
IFN-γ	Interferon gamma
IL-10	Interleukin-10
IL-1β	Interleukin-1β
IL-4	Interleukin-4
IL-6	Interleukin-6
IL-13	Interleukin-13
KC	Kupffer cells
KRH	Krebs-Ringer-HEPES
LC-MS	Liquid chromatography coupled to mass spectrometry
LPS	Lipopolysaccharide
MAFLD	Metabolic-associated fatty liver disease

MAM	Mitochondrial-associated endoplasmic reticulum membranes
Mfn1	Mitofusion 1
Mfn2	Mitofusion 2
MRB	Mitochondrial reaction buffer
MT	MitoTracker™ CMXRos
mtDNA	Mitochondrial DNA
NASH	Non-alcoholic steatohepatitis
NLRP3	NOD-, LRR- and pyrin domain-containing protein 3
NO	Nitric oxide
OCM	One carbon metabolism
OCT	Organic ion transporter
Opa1	Optic atrophy 1
PAMP	Pathogen-associated molecular pattern
PC	Phosphatidylcholine
PE	Phosphatidylethanolamine
PEMT	Phosphatidylethanolamine N-methyltransferase
PFA	Paraformaldehyde
Phos	Phosphocholine
PS	Phosphatidylserine
PVDF	Polyvinylidene difluoride
RIPA	Radio-Immunoprecipitation Assay
ROS	Reactive oxygen species
SAM	S-Adenosyl methionine
TGF β	Transforming growth factor β
TLC	Thin layer chromatography
TLR	Toll-like receptor
TNF	Tumour necrosis factor
TOMM20	Translocase of outer mitochondrial membrane 20
VLDL	Very low-density lipoproteins

Introduction

1.1 The Importance of Choline

Choline is a quaternary amine and vitamin-like nutrient that has three main fates in eukaryotic cells (Figure 1). As a source of methyl groups, choline plays an important role in one-carbon metabolism, as well as a critical component of membrane phospholipids and the neurotransmitter acetylcholine (Jacob et al., 1999; Tucek, 1985; Zeisel, 2012). Choline is a dietary requirement for mammals and can be found in foods such as soybeans, eggs, and liver (Sanders & Zeisel, 2007; Zeisel et al., 2003).

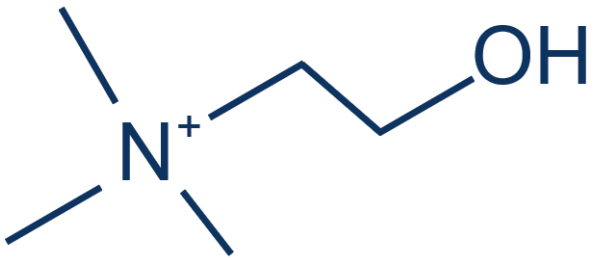

Choline

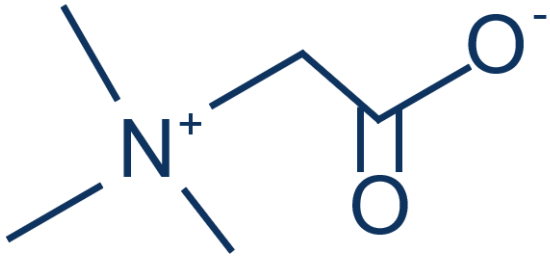

Betaine

Figure 1: Structure of choline and betaine.

One of the first observations as to the importance of choline was made by Charles Best in the 1930s, who found that feeding dogs a raw pancreas, rich in choline, was able to correct a fatty liver (Best & Huntsman, 1935). Mice that have choline removed from their diet showed an increased risk of developing metabolic-associated fatty liver disease (MAFLD, formerly termed non-alcoholic fatty liver disease) (Corbin & Zeisel, 2012). Choline's incorporation into membrane phospholipid phosphatidylcholine (PC), aids in the transport of lipids out of the liver. PC is an important component of very low-density lipoproteins (VLDL) and fat transport (Ghoshal et al., 1983). When choline availability is limited, this creates a decrease in VLDL resulting in the decreased transport of triglycerides from the liver, which causes steatosis (Ghoshal et al., 1983). Since these initial investigations were made, several studies went on to uncover the biological consequences of disrupting choline in diet (Hartroft et al., 1952; Salmon & Copeland, 1954). Further animal models showed that perosis (leg deformities) of chickens is prevented when choline is supplemented (Jukes, 1940). In rats, choline deficiency increased the risk of pathogenesis in blood vessels (Hartroft et al., 1952). In humans, there is an important role in development, where placental transfer of choline enriches neonatal blood with choline compared to adults (Zeisel et al., 1980). The human neonate demand of choline is further highlighted in how rich breast milk is in choline content. In light of this fact, most commercial infant formulas now include the required choline content (Zeisel, 2012). The research done over the past century displays the importance of the essential nutrient choline in a mammalian diet.

1.2 The Role of Choline as a Precursor for Phospholipids

Phospholipids are comprised of a polar head group and two fatty acid side chains esterified to a glycerol backbone (McMurray & Magee, 1972). The head region consists of a phosphate group that is conjugated to choline, ethanolamine, or serine to make PC, phosphatidylethanolamine

(PE) and phosphatidylserine (PS), respectively (Wirtz, 1997). PC is formed *de novo* or from recycling/modification of other phospholipids (Gibellini & Smith, 2010).

Eugene Kennedy in 1956, described a pathway for the synthesis of choline and ethanolamine-containing phospholipids (Kennedy & Weiss, 1956). The Kennedy pathway describes two analogous branches of PC and PE synthesis (Gibellini & Smith, 2010), which produce cytidine 5'-diphosphocholine (CDP) -choline and CDP-ethanolamine, respectively. The two branches share transferase enzyme phosphatidylethanolamine N-methyltransferase (PEMT), which through the addition of three methyl groups converts PE to PC. This conversion of PE to PC occurs primarily in the liver (Gibellini & Smith, 2010). Once choline has entered the cell, choline kinase transfers a phosphate group from adenosine triphosphate, producing phosphocholine and adenosine diphosphate (Fagone & Jackowski, 2013). Next CTP phosphocholine cytidylyltransferase (CCT) adds CTP to produce CDP-choline and an inorganic phosphate (Kent, 1997). In the final step, choline ethanolamine phosphotransferase (CEPT) catalyzes the addition of diacylglycerol (DAG) (Figure 2).

S-Adenosyl methionine (SAM) is a universal methyl donor. In the case of choline oxidation to betaine, which is known to occur in mitochondria of hepatic and renal cells (Grossman & Hebert, 1989; Haubrich & Gerber, 1981), SAM allows for homocysteine demethylation to methionine where PEMT requires three methyl groups to PE to form PC (Kaplan et al., 1993). *Pemt*$^{-/-}$ mice have a normal phenotype compared to controls (Stead et al., 2006; Zhu et al., 2003). However, when choline is removed from the diet, these mice develop NAFLD (Waite et al., 2002) (Vance & Vance, 2009). Therefore, PEMT helps maintain choline pools by *de novo* synthesis during choline depletion.

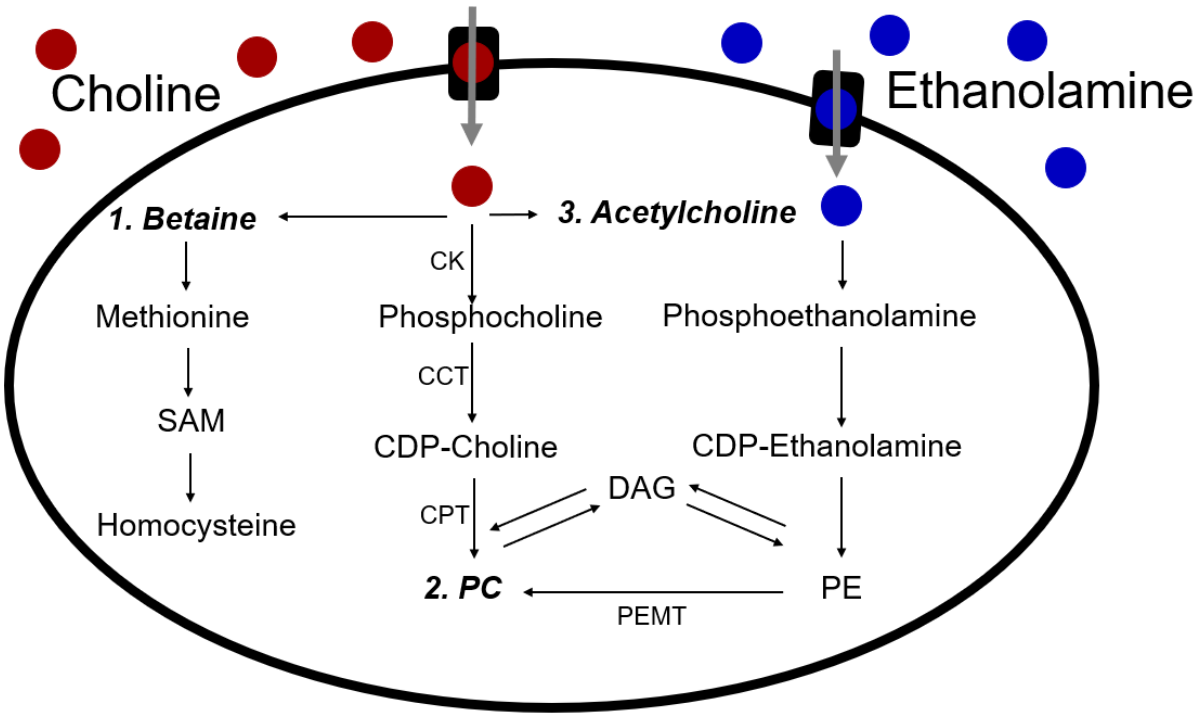
Choline
Ethanolamine
1. Betaine
3. Acetylcholine
CK
Methionine
Phosphocholine
Phosphoethanolamine
CCT
SAM
CDP-Choline
CDP-Ethanolamine
DAG
CPT
Homocysteine
2. PC
PE
PEMT

Figure 2: Fate of Choline in a Cell. The summarized outcomes of choline in a representative cell. (1) Betaine in the methylation pathway. (2) Phosphatidylcholine where CDP-Choline and CDP-Ethanolamine illustrate the two branches of the Kennedy Pathway. (3) Acetylcholine. CK-choline kinase. DAG-diacylglycerol. PC-phosphatidylcholine. Pcyt1- Choline-phosphate cytidylyltransferase N-methyltransferase. PE-phosphatidylethanolamine. PEMT-phosphatidylethanolamine. SAM-S-adenosyl methionine.

1.3 The Role of Choline in Methylation

Betaine (Figure 1) is produced during mitochondrial oxidation of choline to fuel methylation, one carbon methylation (Figure 3) (Kaplan et al., 1993). Choline oxidation primarily takes place in liver and kidney, within the mitochondrial matrix. Choline dehydrogenase (CHDH) resides in the mitochondrial inner membrane where it catalyzes the dehydrogenation of choline to betaine aldehyde (Lin & Wu, 1986). Betaine aldehyde dehydrogenase (BADH) then converts betaine aldehyde to betaine, which exits mitochondria to the cytosol (Brocker et al., 2010; Pietruszko & Chern, 2001). Betaine donates its methyl groups to homocysteine via betaine-homocysteine S-methyltransferase (BHMT) to produce methionine, following which, can be demethylated by SAM (Kaplan et al., 1993). Despite choline flux being characterized in liver and kidney mitochondria, its transport in other tissues remains a knowledge gap.

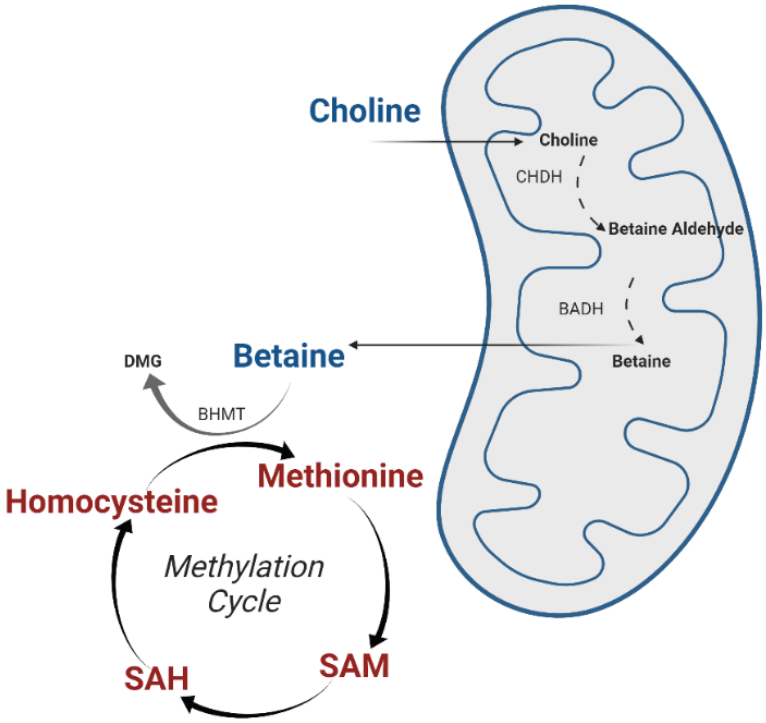
Choline
Choline
CHDH
Betaine Aldehyde
BADH
Betaine
Betaine
DMG
BHMT
Methionine
Homocysteine
Methylation
Cycle
SAH
SAM

Figure 3: One Carbon Metabolism. Choline is converted to betaine aldehyde by dehydrogenation via choline dehydrogenase (CHDH). Betaine aldehyde dehydrogenase (BADH) then converts betaine aldehyde to betaine, which exits mitochondria to the cytosol. Betaine donates methyl groups to homocysteine to produce methionine, which can be demethylated by SAM. S-Adenosylhomocysteine (SAH).

Betaine is a zwitterionic amino acid derivative produced from choline or consumed in foods such as whole wheat, shellfish and spinach (Ueland et al., 2005). Betaine primarily acts as an osmolyte and methyl group donator (Arumugam et al., 2021; Obeid, 2013). In the context of methyl group pools, the relationship between choline, betaine, and folate have been well documented (Niculescu & Zeisel, 2002). Betaine's methyl group can originate from choline or from the B vitamin folate, and be used to convert homocysteine to methionine (Ueland et al., 2005). Folate is a necessary nutrient in mammals, which is required in increased levels during gestation (Willoughby & Jewell, 1966).

Methyl groups are necessary to prevent neural tube defects, but in more general, DNA methylation and protein synthesis, which explains the increased demand in pregnancy (Obeid, 2013; Solé-Navais et al., 2016). Betaine's osmoprotectant properties confer protection against cellular stress, translating to beneficial health outcomes and therapeutic potential in obesity, diabetes, and cancer (Zhao et al., 2018). Mice fed a methionine- and choline-deficient die resulting in MAFLD, supplementing with betaine reduces disease progression and is accompanied by a reduction in oxidative stress and inflammation markers (Veskovic et al., 2019). Furthermore, mice deprived of methyl donors (including choline) that develop MAFLD or non-alcoholic steatohepatitis (NASH), can be rescued with betaine supplementation, highlighting their hepatoprotective role (Veskovic et al., 2019).

1.4 Choline Transporters

Since choline is cationic, it must be shuttled into the cell by a transporter. Three classes of transporters facilitate this process. The first class of transporter is the high affinity sodium-dependent choline transporter (CHT), found on cholinergic neurons (Lockman & Allen, 2002).

CHT moves choline into the cell by ATP-dependent active transport. The second class of transporter is the organic cation transporters (OCT), which are low affinity, ATP- and sodium-independent transporters (Michel et al., 2006). The third group and the focus of this research, is the choline-transporter-like (CTL) family proteins that have intermediate affinity for choline (Traiffort et al., 2013). This specific family of transporter solute carriers (SLCs), are encoded by *SLC44A1-5* transporter genes for the proteins CTL1-5 (Michel & Bakovic, 2009). The CTL1 protein is the product of gene *Slc44a1*. The CTL1 protein was first observed when a yeast triple mutant strain, deficient in the transporter, increased choline transport when transformed with a CTL1 containing plasmid. The addition of exogenous CTL1 protein restored choline transport (O'Regan et al., 2000; Traiffort et al., 2013). The CTL1 protein structure is a nine transmembrane domain protein, containing an N-terminal intracellular domain and a C-terminal extracellular domain (Michel & Bakovic, 2009).

Considerable insight into the role of CTL2 has come from hearing loss and thrombosis research. CTL2 (gene *Slc44a2*) was identified as a 10-1l transmembrane domain protein in humans, and was found to play a pivotal role in antibody-induced hearing loss in guinea pigs (Kommareddi et al., 2007; Nair et al., 2004). CTL2 antibodies have also been linked to autoimmune hearing loss in humans (Beyer et al., 2011). There are 2 isoforms of CTL2 present in seven different tissues types, each with a unique glycosylation pattern and expression, suggesting the potential for varying roles in different tissues (Kommareddi et al., 2010). Antibody-induced hearing loss has been reproduced *in vivo* through antigen binding of the cochlea (Nair et al., 2004). In addition to roles in hearing, the presence of a specific epitope on CTL2 was protective against venous thrombosis. Additional work into thrombotic disease showed that compared to wild-type, *Slc44a2*$^{-/-}$ mice had longer bleed times and delayed thrombosis (Bennett et al., 2020), as well as

disrupted neutrophil function (Zirka et al., 2021). To determine why, *Slc44a2*$^{-/-}$ platelets were isolated and revealed to have dysfunctional mitochondria as noted by low oxygen consumption rates. This dysfunction resulted in lower ADP production, which is necessary for platelet activation. They evaluated if ROS production was altered, as activated platelets require ROS production. It was confirmed that indeed ROS production was affected in *Slc44a*$^{-/-}$ platelets compared to wild-type controls. The level of ROS produced by *Slc44a*$^{-/-}$ platelets matched that of basal cells (Bennett et al., 2020). These experiments showed that when mitochondrial choline demands were not met in *Slc44a*$^{-/-}$ mice, platelets stimulated with thrombin had defective activation (Bennett et al., 2020)

1.5 Choline and Betaine metabolism of Macrophages

Macrophages are a phagocytic member of the innate immune system. Macrophages survey tissue to remove, by phagocytosis, harmful foreign bodies and damaged cells in an organism and combat threats through the production of cytokines (Goerdt et al., 1999; Mosser & Edwards, 2008). Macrophages are also responsible for the clearance of infection, tissue repair, and homeostasis. The various roles of macrophages exist on a continuum, working in tandem with other cells, depending on the need of the host. Following monocyte recruitment and differentiation, macrophages recognize key structures of pathogens called pathogen-associated molecular patterns (PAMPs) and molecules with damage-associated molecular patterns (DAMPs) (Bianchi, 2007). Under classical activation, the well-known PAMP, LPS, stimulates surface Toll-like receptor 4 (TLR4), which trigger a pro-inflammatory response (Martinez, 2011), such as cytokine production, immune cell recruitment, and immune cell activation. Lipopolysaccharide (LPS), tumor necrosis factor alpha (TNFα) and or interferon gamma (IFNγ), binding to their respective receptors, induces the production and secretion of pro-inflammatory cytokines interleukin (IL)-1β, IL-6 and TNFα in

macrophages (Martinez, 2011). M(LPS)s rely on glycolysis to increase ATP production, required for rapid production of reactive oxygen species (ROS) and nitrous oxide (NO) to combat pathogens. In contrast to pro-inflammatory macrophages, alternative interleukin-4 (IL-4) activated macrophages M(IL-4) can differentiate further depending on various humoral responses, needs, and tissue repair requirements (Goerdt et al., 1999). Overall, these cells activate under immunosuppressive conditions such as those conferred by IL-4, IL-13, IL-10, and transforming growth factor beta (TGF β) (Goerdt et al., 1999). M(IL-4) macrophages require the need for new metabolites and therefore favour beta oxidation and oxidative metabolism (Ley et al., 2007). Considering the prevalence of metabolic and inflammatory disease in Westernized societies, discovering new approaches to modulating inflammation has never been more crucial.

In recent years, choline metabolism has been linked to specific immune cell types. Previous work has shown CTL1 to be the main choline transporter in macrophages on the cell membrane, and protein expression of CTL1 increases with LPS treatment (Sanchez-Lopez et al., 2019; Snider et al., 2018). Transport was increased under LPS stimulation in macrophages via an increase in the number of transporters (Meng & Lowell, 1997; Snider et al., 2018). LPS also resulted in increased PC production and an altered cytokine profile. When choline uptake was inhibited with hemicholinium (HC-3, competitive inhibitor of choline transport) or a CTL1 antibody, macrophages adopted an increased proinflammatory phenotype compared to controls in the presence of LPS (Snider et al., 2018). Complementary to this, another group showed a reduction in IL-1β in macrophages when CTL1 expression was inhibited (Sanchez-Lopez et al., 2019). Knockdown of CTL1 decreased choline uptake in macrophages along with mitochondrial ATP synthesis (Sanchez-Lopez et al., 2019).

When macrophages are stimulated with LPS, their activation drives a cascade of inflammatory changes, including cytokine production and an increase in cell volume. The osmolarity compensation required from the increase in volume is controlled in part through betaine (Warskulat et al., 1995; Zhang et al., 1996). Betaine was determined to be a key osmolyte in RAW 264.7 macrophages (Warskulat et al., 1995) suggesting a requirement for betaine availability during activation. In rat livers, macrophage-like Kupffer cells (KCs) induce betaine uptake when exposed to hyperosmotic conditions (Zhang et al., 1996). The lack of choline oxidation enzymes in KCs suggests that choline oxidation to betaine may not occur in KC, suggesting a primarily osmotic role of betaine in these cells (Wettstein et al., 1998).

1.6 Mitochondrial Dynamics

Mitochondria are double-membraned organelles crucial for energy production of the cell. Their double membrane consists of an outer and an inner membrane, which are separated by the inner membrane space (Chinnery & Schon, 2003). Their structure allows for internal housing of protein complexes, which facilitate the production of ATP through oxidative phosphorylation but also other transporters elsewhere in the membrane (Chinnery & Schon, 2003). Key to choline metabolism, choline transporters sit on the outer membrane to allow choline to be shuttled from the cytosol into mitochondria (Pietruszko & Chern, 2001; Taylor et al., 2021). In addition to energy production in macrophages, mitochondria are responsible for the production of ROS, nitric oxide, apoptotic signalling, lipid synthesis and one carbon metabolism (Schmidt et al., 2010; Ueland et al., 2005). The interplay between mitochondria production of ROS and NO to produce bactericidal species as an immune defense highlights a key relationship between macrophages activation and mitochondria. While betaine plays a known role in macrophage osmolarity, the role

of methyl group production in immune cells remains largely unknown. The role betaine plays as an osmolyte in BMDMs activation during cellular stress requires further research.

Mitochondria structures are dynamic given the varying needs of the cell and to maintain mitochondrial health. As mitochondria house their own genome (mtDNA), mitochondrial fission and fusion maintain the health of mitochondria and the cell through metabolite sharing and mixing of mtDNA (Taanman, 1999). While mtDNA houses the genes that produce the machinery required for oxidative phosphorylation, a large portion of mitochondrial genes are located in the cell nucleus (Chinnery & Schon, 2003). Proteins required for one carbon metabolism and choline transporters; therefore, must be trafficked through the endoplasmic reticulum or recruited from the cytosol.

An established role of innate immune cell signalling and mitochondrial-associated endoplasmic reticulum membranes (MAM) is known, where MAMs act as scaffolds to launch immune responses to viral infection (Horner et al., 2011). Pro-inflammatory cytokines trigger innate immune responses by activating the NOD-, LRR- and pyrin domain-containing protein 3 (NLRP3) inflammasome. Co-localization of proteins to the MAM surface activate the pro-inflammatory signalling pathway by controlling the release of cytokines that follow (Zhou et al., 2011).

When macrophages are activated with LPS (during various times in activation), the process of fission occurs more frequently than in naïve cells, which can create distinct fragmented mitochondrial phenotypes (Zezina et al., 2018). In mammals, mitochondrial fission is mediated by Dynamin related protein 1 (Drp1) which constricts mitochondria, collapsing both the inner and outer membrane. Depending on the demand of the cell, mitochondria can readily undergo fission and fusion. Fusion occurs via mitofusion 1 and 2 (Mfn1 and Mfn2) to fuse the outer membranes,

while optic atrophy 1 (Opa1) mediates connection of the inner membranes (Hoppins et al., 2007). ROS production causes cellular oxidative damage, triggering mitochondrial fission and autophagy to recycle damaged mitochondria (Kapetanovic et al., 2020). Given the demands of a proinflammatory macrophage and production of ROS, mitochondrial fragmentation is cell-protective.

1.7 Mitochondrial Choline Transport in Non-Classical Tissues

Mitochondrial CTL1 has been identified in muscle tissue and shown to be sensitive to HC-3 (Michel & Bakovic, 2009). This was the first time, choline transport into mitochondria of non-classical tissue was shown. Recently, CTL2 deficient platelets exhibited impaired mitochondrial respiration (Bennett et al., 2020). Increased oxygen consumption and ATP levels were showed again to be linked to choline metabolism, whereby removal of CTL2 demonstrated impaired, not only ATP production, but ROS mediated platelet activation (Bennett et al., 2020). Being able to better understand the importance of choline uptake and metabolism in activated immune cells would enhance the field of immunometabolism.

2.0 Rationale

Mitochondrial CTL1 was identified in muscle cells (C2C12 myoblasts) and shown to be sensitive to choline uptake inhibition via HC-3, indicating choline transporters may occur in more tissues than originally believed (Michel & Bakovic, 2009). Another group determined CTL2 to be responsible for mitochondrial choline uptake and gatekeeper of activation in platelets (Bennett et al., 2020). Building on previous work in macrophages by Sanchez-Lopez et al., 2019 and Snider et al., 2018, which created the foundation for this work determining that limiting choline transport to M(LPS) alters the immune profile. I aim to establish what biological purpose mitochondrial

choline transport has in macrophages, to examine choline transport and uptake in isolated mitochondria from BMDM of C57Bl/6J mice and RAW 264.7 cells. This approach provides a robust and readily assessable model to further understand how mitochondrial choline metabolism impacts macrophage biology.

3.0 Hypothesis

Mitochondrial choline transport occurs in macrophages under the control of CTL2 and increases with LPS activation.

4.0 Objectives

4.1 Objective 1 - Interrogate mitochondrial choline transporter localization in macrophages.

To confirm the presence of CTL1 and/or CTL2 on the mitochondrial membrane, pure mitochondrial fractionations were isolated to detect these proteins by Western blotting (Figure 4). Both BMDMs and RAW 264.7s treated ± LPS were used to detect choline transporter localization. Additional cell types were used as controls and troubleshooting models.

4.2 Objective 2 - Characterize mitochondrial choline uptake.

To determine if and how active choline transport is affected by inhibition with the known choline uptake inhibitor HC-3 and if the presence of immune stimuli are important, I sought to track mitochondrial choline uptake in isolated mitochondria in naïve and M(LPS)s. Mitochondria were isolated in a crude fractionation, allowing for transport to be tracked using radiolabelled ^{3}H-choline (Figure 4).

4.3 Objective 3 - Decipher the downstream role of mitochondrial choline metabolism.

BMDMs from C57BL/6J mice were isolated and used to determine how different conditions affected metabolites up and downstream of one carbon metabolism (Figure 4). Targeted metabolomics was conducted on cells treated with the following four conditions: naïve, choline deprived (via media lacking choline or choline transport inhibition), LPS treated, and IL-4 treated. The aim was to be able to determine if challenging choline uptake alters the total pool of cellular betaine and other key metabolites.

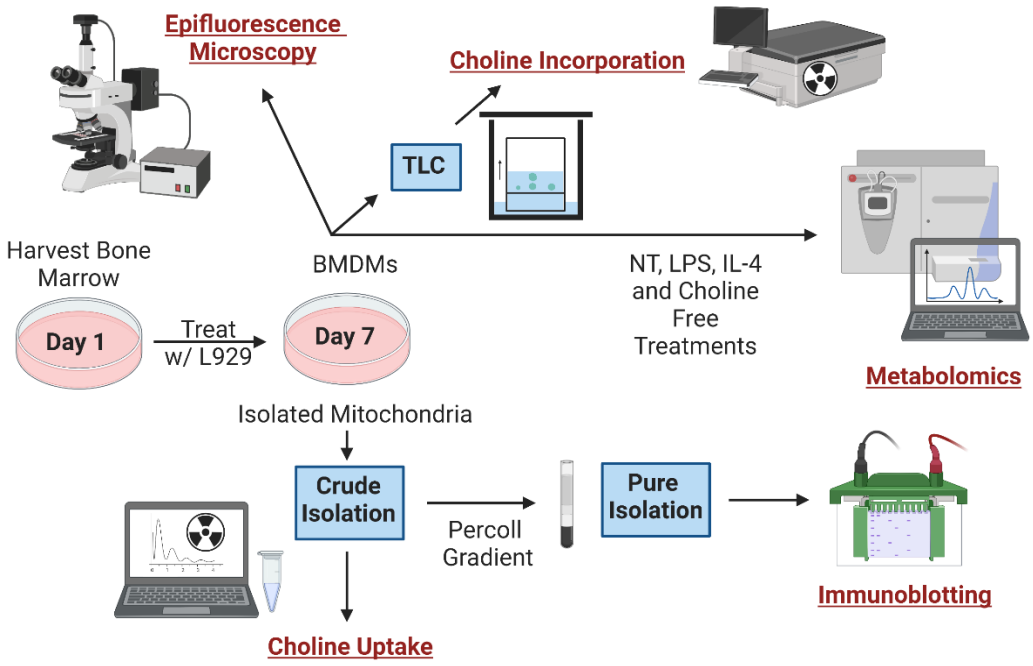
Epifluorescence Microscopy
Choline Incorporation
TLC
Harvest Bone Marrow
BMDMs
NT, LPS, IL-4 and Choline Free Treatments
Day 1
Treat w/ L929
Day 7
Metabolomics
Isolated Mitochondria
Crude Isolation
Percoll Gradient
Pure Isolation
Immunoblotting
Choline Uptake

Figure 4: Project experimental methodology. Analysis follows five experimental outputs. Three are from whole cell: epifluorescence microscopy, choline incorporation, and metabolomics. Two methods utilize isolated mitochondria: immunoblotting and choline uptake.

5.0 Methods

5.1 Cell Culture and Mice

Using male WT C57BL/6 on regular chow diet aged 15-30 weeks, bone marrow was isolated and cultured to produce bone marrow-derived macrophages. Mice were anesthetised using 0.1 ml isoflurane gas and euthanized with cervical dislocation. The tibia and femur were isolated from surrounding tissue, dislocated at the hip and separated. Bones were placed in PBS on ice. Bones were washed with 70% ethanol for 10 seconds and rinsed with PBS before cutting the distal ends of the bone to expose marrow. Bones were then placed distal end down in a 0.5-ml Eppendorf tube with a hole in the bottom punctured by an 18-gauge needle that was placed inside of a 1.5-ml Eppendorf tube. 100 μL of cell culture media (Dulbecco's modified eagle medium **(**DMEM) [Multicell 1X MOD. #319-005-CL] with 10% FBS and 1% penicillin/streptomycin) was added to the tube. Tubes were spun at 1500 g for 5 min to pellet bone marrow. Pellet and supernatant were resuspended in cell culture media and pipetted over a 0.22 μm filter to remove contaminates. Cells were cultured in 20 mL of 20-25% L929 cell culture media on a 15-cm dish and allowed to differentiate and adhere for 6-7 days. On Day 3 post-isolation, cell culture dishes were topped up with 5ml of 20-25% L929 supplemented cell culture media. Dishes were incubated at 37°C and 5% CO_2.

The bone marrow culture was supplemented with supernatant from L929 cells which produces growth factor, macrophage colony stimulating factor (M-CSF). Conditioned media was produced by culturing L929 cells in Dulbecco's modified eagle medium for 10 days (DMEM with 4.5 g/L of glucose, with L-glutamine and sodium pyruvate, Wisent) supplemented with 10% fetal bovine serum (FBS, heat-inactivated, Wisent) and 1% penicillin/streptomycin (Fisher). Cells were spun out of culture at 3000 rpm and the resulting supernatant filtered (0.22 μm). Dishes were

washed once with room temperature PBS, then 10 mL of 4°C 10 mM EDTA in PBS was added to the dish and placed on a cold fridge shelf at 4°C for 8-10 min. Cells were lifted from the dish using a 10 ml pipette and repeating pipetting. Cells were added to a 15-ml Falcon tube and spun at 400 g for 5 min to pellet cells. Cells were resuspended in cell culture media or washed once with 10ml of PBS to preform mitochondrial isolation assays.

RAW 264.7

Frozen stocks of RAW 264.7 (ATTC), a macrophage like mouse cell line, were stored in liquid nitrogen in 1 mL of 10% DMSO FBS were quick thawed by adding 1 mL of cell line media (DMEM with 10% FBS and 1% penicillin/streptomycin with 100ug/ml Normocin 37°C). Cells were resuspended in a total of 10 ml of cell culture media and spun at 400 g for 5 min to remove DMSO. The resulting cell pellet was resuspended in cell line media and placed in a 175 cm^3 T-flask until 75% confluent. Cells were checked every 24 h. If the culture exceeded 3 days, the culture was topped with 5 mL of cell culture media. Flasks and dishes were stored at 37°C and 5% CO_2. Once 75% confluent, cells were split into 15-cm dishes for the remainder of the cell culture until 80% confluent. RAW 264.7s were lifted using a 25 cm scrapper. Dishes were washed with 10 mL of room temperature PBS and scraped in 10 mL of PBS (for mitochondrial isolation) or cell line media for immunofluorescence (IF).

C2C12

Frozen stocks of C2C12s, an immortalized mouse myoblast cell line was stored in liquid nitrogen in 1 ml of 10% DMSO 50% FBS 50% supplemented DMEM were quick thawed by adding 1 ml of cell line media 2 (DMEM with 20% FBS and 1% penicillin/streptomycin with 37°C). Cells were resuspended in a total of 10 ml of cell culture media and spun at 400 g for 5 min

to remove DMSO. The resulting cell pellet was resuspended in cell line media 2 and placed in a 175 cm^3 T-flask until 60-75% confluent. Cells were checked every 24 h. If the culture exceeded 3 days, the culture was topped with 5 mL of cell culture media 2. Flasks and dishes ware stored at 37°C and 5% CO_2. Once 75% confluent, cells were split into 15-cm dishes for the remainder of the cell culture until 80%, at which point they were lifted for assays. C2C12s were lifted using trypsin (0.05%/EDTA 0.53 mM: Wisent 325-042-CL). Dishes were washed with 10 mL of room temperature PBS and lifted with 8-10 ml of trypsin. Flasks and dishes were incubated at 37°C for 6 min and cells were lifted with repeat pipetting. Suspended cells were added to a 15-ml Falcon tube and spun at 400 g for 5 min for remove trypsin. Cells were resuspended in cell culture media for IF.

Hepatocytes

Hepatocytes were isolated from C57BL/6J mice. Mice were female, aged 24 weeks and fed a chow diet. Mice were anesthetized, the upper vena cava was clamped, the portal vein snipped, and the lower vena cave was clamped with a suture knot. Liver was perfused through the lower vena cava with 25 ml of EGTA at a flow rate of 7 ml/min. Following flushing, 25 ml of collagenase solution (Sigma; cat # C5138: 0.5 mg/mL Collagenase Type IV in HEPES buffer: 66.7 mM NaCl, 6.7 mM KCl, 4.8 mM $CaCl_2 \cdot 2H_2O$ and 0.1M HEPES) was perfused into the liver at a flow rate of 6 ml/min. Liver was mechanically separated with scissors in a sterile Petri dish with 10 ml Williams' Media E (Basal- no FBS, Antibiotics or L-Glut). Liver cells were released from capsule with fine forceps. Cells were transferred to a new 15-mL tube with a 100 μM cell strainer. Cells were split into 2 portions and spun at 400 g for 4-5 min. Supernatant was discarded and cells were resuspended in 10 ml of basal media, then spun at 400 g for 4-5 min. Final cell pellet material was resuspended in 10 ml of complete media (Williams' media with 10% FBS and 1%

antibiotic/antimycotic mixture). Trypan blue exclusion method was performed to determine percent viability. Cells were plated at 55,000 cell per well on collagen (0.01% collagen in 0.2% acetic acid) pre-coated glass microscopy slides (ibidi: 81201). Cells were incubated for 3 h, washed with PBS to remove dead cells, and incubated overnight at 37°C and 5% CO_2. This isolation was performed by Conor O'Dwyer.

5.2 Mitochondrial Isolation

Crude mitochondrial isolation

Cells were washed and pelleted in PBS and placed on ice for the remainder of the isolation. Cells were from culture unless otherwise specified where a freeze thaw cycle was performed prior to isolation. A minimum of $30x10^6$ BMDMs or $20x10^7$ RAW 264.7 cells were used per isolation. The cell pellet is resuspended in 1 mL of in house made Buffer A (Buffer B with 2 mg/mL BSA). The sample was then transferred to a glass-glass homogenizer (Kimble 15 ml tissue grinder: 885300-0015) and the 4 mL Buffer A was added. A total of 15-20 strokes were performed with the loose pestle. A total of 60-75 (60 from frozen, 75 from fresh cell culture) strokes were performed with the tight pestle. Buffer B (220 mM mannitol, 70 mM sucrose, 20 mM HEPES (pH 7.4), 1 mM EDTA, 1 Sigma protease cocktail inhibitor tablet [11083580001] per 250ml of buffer). This protocol was adapted from Yan Burelle's group, University of Ottawa (Cuillerier et al., 2021).

Crude mitochondria isolation version 2A

Homogenate was transferred to a Nalgene (Thermo, Nalgene, Oak ridge centrifuge clear: 3118-0050) centrifuge tube and resuspended in 30mL with Buffer A. Samples were spun twice at 1000 g for 10 min at 4°C, discarding the pellet each time. The supernatant was transferred to a new Nalgene tube and spun at 10,000 g at 4°C for 10 min. The supernatant was discarded, and

pellet resuspended in 30 mL Buffer B. Samples were spun for 10 min, 10,000g at 4°C. The last two steps were repeated to wash the pellets. Final pellets were resuspended in 200 uL Buffer B.

Crude mitochondria isolation version 2B

All tubes were prewashed in Buffer B. Homogenate was transferred to 15-ml Falcon and topped to 15 ml of Buffer B. Samples were spun at 800 g for 5 min at 4°C. This step was performed twice more with the resulting supernatant to pellet out cell debris. The supernatant was transferred to a new Nalgene tube and spun at 10,000 g at 4°C for 10 min. The supernatant was discarded, and pellet resuspended in 30 mL Buffer B. Samples were spun for 10 min, 10,000g at 4°C. The last two steps were repeated to wash the pellets. Final pellets were resuspended in 200 uL Buffer B.

Pure Percoll gradient

Ultracentrifuge tubes (Beckman Coulter #331372) were prepared by pouring 8 mL of Percoll solution into the tube (30% Percoll [sigma P4937], 225 mM mannitol, 25 mM HEPES [pH 7.4], 1 mM EGTA). Crude mitochondria are layered on top of the Percoll solution, without mixing the two. 3 mL of mitochondrial reaction buffer (MRB:250 mM mannitol, 5 mM HEPES [pH 7.4], 0.5 mM EGTA) was layered on top of crude mitochondria and volume completed to approximately 3.5 ml of MRB after adjusting to precisely balance the tubes for centrifugation. The samples were spun at 95,000g (24,000 rpm) in a Beckman L-100XP ultracentrifuge with Beckman SW41Ti singing bucket rotor (09E100) for 30 min at 4°C, maximum acceleration. Top layers were removed with a P1000 pipette to remove contaminants. The mitochondria fraction corresponding to the thin line near the bottom of the tube was removed with a P200. Mitochondria were then transferred to a 1.5-mL Eppendorf tube and resuspended in 1.5-mL of MRB. Suspension was divided into 4 1.5-mL tubes, topped to 1.5-mL and pipette mixed to wash out Percoll. Tubes were spun at 16,400 g

for 10 min at 4°C. Supernatant was discarded and resulting pellets were combined and washed with 1.5-mL of MRB then the previous spin was repeated. Supernatant was removed to approximately 25 μL and 25 μL of denaturing radio-immunoprecipitation assay (RIPA) buffer **(**25 mM Tris-HCl pH 7.6, 150 mM NaCl, 5 mM EDTA, 1% NP-40 [IGEPAL CA 360], 1% sodium deoxycholate and 1 Sigma protease cocktail inhibitor tablet [04693159001]) was added to the sample. Bradford assay was performed, and samples stored at -20°C.

5.3 Western Blotting

Pure mitochondrial pellets were obtained from BMDM and RAW 264.7 (cells polarized with LPS [100 ng/mL] for 24 h prior to cell isolation. Mitochondrial pellets were suspended in 50% MRB: 50% RIPA. A Bradford protein assay was performed to determine protein concentration. Denaturing loading dye was added to the sample and then boiled for 5-10 min at 95°C. The sample was loaded into a 12% SDS-PAGE gel or BIO-RAD Mini-Protean TGX Gels 4-20% where it ran for the specified amount of time (average 120 min) at 120V. Gel was then transferred onto a PVDF (polyvinylidene difluoride) membrane (19 min 1.3 A) using a Trans-Blot® Turbo™ Transfer System (Bio-Rad) with Bjerrum Schafer-Nielsen buffer (48 mM Tris, 39 mM glycine, 20% methanol) onto a PVDF membrane activated with methanol. The membrane was blocked for 1 h with 5% BSA. Membrane was cut at appropriate locations and the sections were placed with primary antibodies at 4°C overnight: CTL1 21: SLC44A1 Rabbit Polyclonal Antibody: 21279-100 (Cedarlane), CTL2: Anti-SLC44A2 Rabbit Antibody: A05467-1 (Cedarlane), B actin: beta-Actin (13E5) Rabbit mAb HRP Conjugate 5125S (Cell Signalling Technology), Histone 3: Histone H3 (D1H2) XP (R) Rabbit mAb HRP Conjugate 16648S (Cell Signalling Technology), TOM20: AntiTOMM20 Mouse mAb H000009804-M01 (Abnova), and ATPase: Na, K-ATPase 1 Rabbit Ab 3010S (Cell Signalling Technology). Antibodies were

suspended at a dilution of 1/1000 in 5% BSA. The next day, membranes were washed four times in TBST (20 mM Tris, 150 mM NaCl, 0.05% Tween® 20). Membranes were then placed in secondary Anti-rabbit IgG HRP-linked Antibody (Cell Signalling Technology 7074S) or Anti-mouse IgG HRP-linked Antibody (Cell Signalling Technology 7076S) as appropriate and then washed four times in TBST**.** Membranes were activated with Clarity™ Western ECL solution (BioRad) and protein bands visualised with LAS 4010 ImageQuant Imaging System (General Electric) or ChemiDoc™ MP Imaging System (BIO-RAD). Band contrast was adjusted using ImageJ software.

5.4 Choline Uptake

Whole cell choline uptake assays were performed with ^{3}H-choline chloride (Perkin-Elmer). Krebs-Ringer-HEPES Buffer (KRH, 130 mM NaCl, 1.3 mM KCl, 2.2 mM $CaCl_2$, 1.2 mM $MgSO_4$, 1.2 mM KH_2PO_4, 10 mM HEPES, pH 7.4, and 10 mM glucose) was filter sterilized (0.22 μM). ^{3}H-Choline solution was made to a final concentration of 1 μCi/mL in KRH buffer with 2% glucose (F/S KRH). BMDMs (day 6) were plated at a concentration of 2 million per 6 well dish, 24 hr before treatment. The following day, cells were washed with room temperature PBS and 300 μL of F/S KRH buffer was added to plates. Cells were incubated for 1 h at 37°C. KRH buffer was aspirated off, the 300uL of 1uCi/mL ^{3}H-Choline solution was added and samples were incubated at 37°C for 30 min. ^{3}H-Choline solution was removed, washed once with KRH buffer and 150 μL of NaOH was added and plates were frozen at -80°C for radiolabeled counting.

Mitochondrial Uptake Method 1: Simple suspension

Crude mitochondrial isolation was performed. The sample was suspended in mitochondrial uptake buffer (120 μM KCl, 5 μM HEPES/KOH, 1 μM EGTA, 5 μM KH_2PO_4, 0.5 μM $MgCl_2$, 5 μM L-glutamate, and 1.2 μM L-malate, pH 7.2) on ice. A portion of suspension was taken to

quantify protein via Bradford assay. Mitochondria were spiked with 10 μCi ^{3}H-Choline/mL and Hemicholinium-3 (HC-3: Sigma H108-500MG, 50, 100, 250, and 500 μM) RSM932A (RSM: Cayman Chemicals, 1 and 5 μM) for 5 min at 22°C. Mitochondria were pelleted for 5 min at 10,000g at 4°C. Sample was washed with 1 mL of uptake buffer and pelleted again. Supernatant was removed, and pellet was resuspended in NaOH and frozen for radioisotope counting.

Method 2: Oil layering

Crude mitochondrial isolation was performed. The sample was suspended in mitochondrial uptake buffer 1.6 μM ADP. A portion of suspension was taken to quantify protein via Bradford assay. In 1.5 μL tubes, 100 μL of lysis buffer (250 mM sucrose with 2% Triton X-100) was added. 350 μL of oil mixture (58% Dinonyl phthalate [Sigma] and 42% Silicon fluid DC550 [Sigma]) was layered on top. Mitochondria were suspended in experimental buffer (Mitochondrial uptake buffer, with ADP and 10 μCi/mL ^{3}H-Choline) made to 100 μL of volume and added into oil mixture to create a bubble of buffer in the oil (Figure 12). Experiment was run in technical duplicates. Tubes were placed at 22°C for 5 min and then spun at 12,500g for 2 min to pellet mitochondria. A portion of the reaction bubble, oil layer, and all of the lysis buffer was collected for radiolabel counting. This protocol was adapted from Patten et al., 2021.

Radiolabel Counting

Samples were added to 4 ml of PerkinElmer ULTIMA GOLD™ MV scintillation fluid and read with a on PerkinElmer beta-scintillation counter (Tri-Carb 2910TR). Scintillation vials were vortexed at high speed to resuspend mitochondrial pellets into scintillation fluid and left overnight before samples were read. The amount of uptake was displayed as disintegrations per minute (DPM) per μg of protein.

5.5 Choline Incorporation

BMDMs (day 6) were plated at a concentration 2 million per 6 well dish or 5 million for 10 cm dish, 24 h before treatment. The following day, cells were washed with room temperature PBS and 1 µCi/ml of ^{3}H-choline chloride (Perkin Elmer) was added as per time points (2, 4, 6, 8, and 24 h). Cells were washed with PBS and 2 mL of PBS was added to dishes and dishes were placed at -80°C.

Bligh and Dyer assay was performed from 200 µL of cell suspension, homogenized in 750 µL of chloroform:methanol (1:2). Samples were vortexed for 15 secs and incubated on ice for 20 min. Next, 250 µL chloroform and 250 µL H_2O were added and tubes shaken vigorously to ensure the phases were fully mixed. Tubes were centrifuged for 5 min at room temperature at 3,000 rpm. The top aqueous phase or bottom lipid was removed and placed into a new tube. The aqueous phases were concentrated using nitrogen evaporation. Concentrate was resuspended in 50:50 ethanol:water (aqueous) or 50:50 chloroform:water (lipid) and stored at -20°C.

Using Millipore TLC Silica gel 60 (20 cm), 1.5 cm lanes were created using an 18-gauge needle. Scored plates were then baked for 1 h at 100°C or 30 min at 200°C and stored at room temperature until used. The aqueous solvent for thin layer chromatography (TLC) contained 50:25:5 MeOH:saline:NH_4OH and lipids solvent 65:32:4 $CHCl_3$:MeOH: H2O for a total of 100 ml. Solvent was added to the glass chamber while samples were loaded to plates. 25 µL of standard; Betaine (Sigma: 61962-50G), Phosphocholine (Sigma:P0378-5G), Phosphatidylcholine (Sigma: P3556-100MG), free choline (BioShop: CHO386), CDP-choline (Sigma:C0256) or the sample was added to each lane, spotted with a Hamilton Syringe. After all samples were spotted, the plates were allowed to full dry before placing them in the chamber. Plates were added to the chamber to form full horizontal contact with the solvent and plates were allowed to run until 5 cm

from the top of the plate and solvent front was marked. The plates air dried in a fume hood to evaporate off solvent, once dry, the plates were added to a new glass chamber with iodine for sample visualization.

The silica pertaining to each sample was added to 4 ml of PerkinElmer ULTIMA GOLD™ MV scintillation fluid and read with a on PerkinElmer beta-scintillation counter (Tri-Carb 2910TR). Incorporation displayed as DPM per μg of total cell lysate protein.

5.6 Microscopy staining and fixation

Microscopy method 1:

Hepatocytes were plated in ibidi 12 Well chamber, removable slide (81201) at a concentration of 55,000 cells per collagen coated well. Wells were incubated at 37°C and 5% CO_2. Fixation performed at room temperature. Wells were washed with filtered (0.22 μm) PBS three times. Then 300 μL of 4% paraformaldehyde in PBS (PFA) was added to each well and incubated for 20 min and washed twice. Cells were permeabilized for 5 min in permeabilization solution (0.1% Triton X-100 and 0.5% BSA in PBS). Wells were washed once with PBS. Cells were then blocked for 20 min with blocking solution (0.1% Triton X-100 and 5% BSA in PBS). The blocking solution was removed without washing and primary antibodies in permeabilization solution were added at a concentration of 1:100 [CTL1 21: SLC44A1 Rabbit Polyclonal Antibody: 21279-100 (Cedarlane), CTL2: Anti-SLC44A2 Rabbit Antibody: A05467-1 (Cedarlane), and TOM20: AntiTOMM20 Mouse mAb H000009804-M01 (Abnova)]. The wells were washed twice and Anti-Mouse IgG (H+L) Highly Cross-Adsorbed Alex Fluor 488 (Fisher Scientific A11001), and Anti-Rabbit IgG (H+L) Highly Cross-Adsorbed Alex Fluor Plus 647 (Fisher Scientific PIA32733) secondary antibodies were added at a concentration of 1:1000 in permeabilization solution and incubated for 1 h. Wells were washed twice and DAPI was added at a concentration of 14.3 μM

in PBS for 5 min. Wells were washed once and all solutions were removed. The chamber divider was removed and 40 µl of Thermofisher Prolong Gold Antifade Mountant then a Corning 1.5 Cover Glass 2980-245. The coverslip was sealed on the corners and let to stand for 10 mins. The edges of the coverslip were then sealed with clear nail polish and allowed to cure for 30 min. Slides were then stored at 4°C in the dark until image acquisition.

Microscopy method 2:

BMDMs were plated in chamber slides at a concentration of 55,000 cells per well on day 6 or 7. Cells were allowed to adhere for 24 h before fixation in cell culture media with or without 100 ng LPS treatment. RAW 264.7 (P.20) with or without 100 ng LPS treatment and C2C12s (P.14) were plated at 15,000 and 10,000 cells respectively in cell culture media and allowed to adhere for 24 h. Wells were incubated at 37°C and 5% CO_2 all treatments were conducted at 37°C until post fixation. Slides were placed on top of a T-75 flask filled with water and pre-warmed at 37°C until fixation. All washes were done with PBS. Wells were washed with filtered (0.22 µm) PBS three times. Wells received 300 µL of cell culture media with or without 150 nM MitoTracker™ CMXRos (Thermofisher), at which point wells were kept under aluminum to prevent light exposure for remainder of the protocol. 300 µL of 4% PFA was added to each well and incubated for 20 min and washed twice. Cells were permeabilized/blocked for 30 min in PB solution (0.5% Triton X-100, 1% BSA in PBS). PB solution was removed without washing and primary antibodies 50% PB solution in PBS concentration of 1:100 was added to the wells for 1 h (C-term: Fullerton Lab Homemade CTL1 C-terminus-3 1.47 mg/mL (BioBasic), CTL1 14: SLC44A1 Rabbit Polyclonal Antibody: 146871-AP (Cedarlane), and CTL2: Anti-SLC44A2 Rabbit Antibody: A05467-1 (Cedarlane). Wells were washed three times then secondary antibody Goat Anti-rabbit Highly Cross-Adsorbed Oregon Green 488 (LifeTech O11038) was added at a concentration of

1:1000 in 50% PB solution in PBS and incubated for 1 h. Wells were washed three times and DAPI was added at a concentration of 14.3 µM in PBS for 5 min. Wells were washed once and all solutions were removed. The chamber divider was removed and 40 µL of Thermofisher Prolong Glass Antifade Mountant then coverslip (Corning) was added. The coverslip was sealed on the corners and left to cure overnight. Slides were then stored at 4°C in the dark until image acquisition. Protocol was adapted from steps provided by Julia St-Pierre's group at the University of Ottawa.

5.7 Image acquisition and Processing

Initial microscopy imaging was performed using the Zeiss Axio-Observer Z1 inverted widefield microscope driven by Zen 2.6. The microscope was outfitted with the Zeiss AxioCam HRmono camera, the X-cite Xylis LED light source and the plan Apochromat 63x/1.4 NA (used in combination with the Zeiss oil immersion 518F). The detection of the different fluorophores were sequential as follows: Mitotracker CMxROS: Filter: Ex 545/30 nm, FT570 nm, Em 620/60 nm, exposure time: 250 ms, Light intensity: 15 ms Oregon green channel: Filter: Ex 470/40nm, FT 495 nm, Em 525/50 nm, exposure time: 200 ms, Light intensity: 15%. DAPI: Ex G365, FT. 395 nm, Em 420 nm LP, exposure time: 20 ms, Light intensity: 12%. Original images were processed with Zen 2.6 (Blue Edition) Fast Iterative deconvolution (strength 4.03), 6 iterations per channel, with bad pixel and background corrections applied. Hepatocytes were imaged with similar settings, but exact channel settings not shown here.

To improve resolution, microscopy was performed on a Zeiss Axio-ObserverZ1-LSM 880-AiryScan confocal microscope driven by the Zen Black 2.3 software. The Laser Scanning microscope is outfitted with a Plan Apochromat 63x objective, used in combination with the Zeiss Immersion oil 518F. High resolution images were captured using the AiryScan detector

(sequential, unidirectional scanning at a frame rate of 3.6 s, pixel size of 0.05 mm, z-stack of 0.2 mm slice thickness). DAPI, Oregon Green (CTL1 or CTL2) and MitoTracker™ CMXRos, were excited using the diode laser 405 nm (1.5%), the Argon laser at 488 nm (3%) and the diode laser 561 nm (3%) respectively. The fluorescence from DAPI and Oregon Green, was detected using a BandPass (BD) filter of BP420-480 + BP495-550 and setting the master gain of the detector at 700 and 800 respectively. MitoTracker fluorescence was filtered by a BD filter BP570-620 + LP645 before being detected by the AiryScan with a master gain set at 800. Raw images went through Airyscan processing before being used for the surface rendering.

Surface rendering was performed using Imaris 9.9.1 (Bitplane, Oxford Instruments), with the following settings: Background subtraction LS (Diameter of the Largest Sphere) set at: 0.25 mm, without smoothing, objects smaller than 30 voxels were filtered out. Object-Object statistics option was selected from the beginning, providing the volume of the overlapping voxels (unit in 3D) between mitochondria and the protein of interest (CTL1 or CTL2). Overlapping voxel were displayed in yellow and the ratio between the volume of mitochondria containing CTL signal to mitochondrial volume shown.

Statistical analysis was performed using GraphPad 9. The ratio of colocalization to mitochondrial volume was analyzed using a two-way ANOVA with Sidak's multiple comparisons test which compared antibody stain to treatment. Statistical significance is noted as follows: * $p < 0.05$, and **** $p < 0.0001$, 95% confidence interval.

5.8 Metabolomics

BMDMs were cultured following cell culture methods for 6 d in 15 cm dishes and then isolated or added to 10 cm dishes on day 6. Dishes were washed with 5 mL of room temperature PBS and

then treatments were added in 20 mL of cell culture media and incubated at 37°C and 5% CO_2 for 24 h. Choline-free media was prepared with DMEM w/o choline (US Biologicals: D9809), supplemented L-methionine (Sigma: M5308), D-pantothenic acid hemi-calcium salt (Sigma: P5155), *myo*-inositol (Sigma: I7508), sodium pyruvate (Sigma: P2256), and 2 mM Glutamax (ThermoFisher: 35050-061), and sodium bicarbonate to match our standard DMEM formulation, then adjusted to pH 7.1-7.2. Solutions made with sterile molecular biology grade water. Media was filtered using Nalgene™ Rapid-Flow™ Sterile Filter Storage Bottles (ThermoFisher:455-0500) with Nalgene™ Rapid-Flow™ Sterile Disposable Bottle Top Filters with PES Membrane (ThermoFisher:09-741-07). Treatments included choline-free media, hemicholinium-3 (HC-3, Sigma H108-500MG, 250 µM), LPS (from *E. coli:B4*, Sigma-Aldrich, 100 ng/ml), and IL-4 (mouse recombinant IL-4, R&D, 20 ng/mL) for 24 hr.

Two separate experiments were performed on separate days and samples pooled together for metabolic profiling. Dishes were removed from the incubator and placed on ice following washing with all reagents and tubes on ice or from the freezer. The media was removed, and dishes were washed three times with at least 3 ml of ice cold 150 mM ammonium formate solution (150 mM ammonium formate, pH was adjusted at 4°C to 7.4 using NH_4OH). This was followed by the addition of 400 µL of 50% MeOH/ 50% LC/MS-grade water solution. The dishes were scraped and added to a pre-chilled 2 mL bead beater tube (Eppendorf Cat# 022363352) with 6-7 washed ceramic beads inside (1.4 mm Omni International, PN: 19-645-3). The dish was washed with 200 µL of 50% MeOH/50% water solution and added to the tube. Tubes were vortexed for 10 s, followed by the addition of 220 µL of acetonitrile and vortexed once more and stored on dry ice. The samples were homogenized using the Roche MagNA Lyser at 2000 rpm for 60 s, the plate and samples were placed on dry ice for 1 min and then repeated. 600 µL of ice-cold

dichloromethane and 300 µL of ice-cold H_2O were then added to the tubes and vortexed for 30 s and left to partition on ice for 10 min. The samples were spun at 4,000 g at 1°C. The upper water-soluble metabolites were collected in a new tube on dry ice and dried using a refrigerated CentriVap Vacuum Concentrator at -4°C (LabConco Corporation, Kansas City, MO). Samples were stored at -80°C until ready for LC-MS/MS data collection. This protocol was provided by the University of Ottawa Metabolomics core.

Choline pathway metabolites were quantified by Dr. Shama Naz who optimized the quantification acquisition method using liquid chromatography coupled to mass spectrometry (LC-MS). All samples were temperature-controlled and all MS-grade solvents pre-equilibrated to -20°C. Samples were resuspended with 75% acetonitrile, cleared by centrifugation and then run on an Agilent 6545B Q-TOF mass spectrometer equipped with a 1290 Infinity II ultra-high performance LC (Agilent Technologies). Continuous internal mass calibration was executed using signals from purine [12,000 full width at half maximum (FWHM) resolution] and hexakis (^{1}H, ^{1}H, ^{3}H-tetrafluoropropoxy) phosphazine (24,000 FWHM resolution). All study samples were randomized before analysis and run using both high and low pH hydrophilic interaction chromatography (HILIC-Z) in negative and positive ionization mode respectively. HILIC separation was obtained using the Poroshell 120 HILIC-Z column (2.1, 100 mm, 2.7 mm; Agilent). The chromatographic conditions and mass spectrometry acquisition parameters were performed as previous described (Menzies et al., 2021). Metabolite identification was confirmed by exact mass, retention time and subsequent MS/MS fragmentation of metabolite standards. The metabolites were quantified (relative quantification) by external standard calibration curves with Mass Hunter Quant (Agilent). Metabolite concentrations were recorded as µM per million cells.

6.0 Results

6.1 Detection of CTL Proteins in Mitochondrial Fractions

To determine if CTL1 or CTL2 could be detected on the mitochondrial membrane, I first sought to determine if the proteins were present in pure mitochondrial fractions. Several different centrifugation techniques were trialed using BMDMs and immortalized macrophages. These techniques were optimized to strive for a "pure" fraction. While a completely pure fraction is rather challenging to obtain, some trials of the ultracentrifugation in RAW 264.7 which started with higher cell numbers and had more effective initial contaminant removal, proved to be more effective than other methods. As CTL1 is known to be present on the plasma membrane of macrophages, a cell membrane (Na+/K+ ATPase) marker was used to identify the purity of the mitochondrial fraction post-centrifugation. Additionally, cytosolic and nuclear contamination was monitored with β-Actin and Histone-, respectively. A marker of translocase of outer mitochondrial membrane 20 (TOMM20) was used to probe for mitochondrial enrichment of isolated fractions. While one trial of isolating a pure mitochondrial fraction from RAWs was devoid of cytosolic, nuclear, and cell membrane contaminants (Supplementary Figure 1), following trials failed to demonstrate this level of purity in either BMDM or RAW (Figure 5 and 6). The initial pilot probing for CTLs in C2C12s using the current centrifugation methods additionally provided to be inconclusive (data not shown).

CTL2 was detected in both the whole cell lysate and the mitochondrial fraction in RAW 264.7s treated ± LPS (Figure 5). These fractions were enriched for mitochondria compared to whole cell lysate as determined by TOMM20, but a notable presence of cytosolic contamination and some cell membrane contamination was detected. All mitochondrial fractions were devoid of nuclear contamination (Figure 5). In Figure 6, lanes 2 (NT) and 8 (LPS) show the presence of CTL2 and

TOMM20, with reduced cytosolic contamination and elimination of cell membrane or nuclear contaminants in mitochondrial fractions from BMDMs (Figure 6). Detecting CTL1 by Western blotting has proved challenging. The Fullerton lab found previously that antibody detection is optimal under non-denaturing conditions; however, this was not conducive to this experimental design. While faint bands in RAW 264.7s (Figure 5) that may correspond to CTL1 are apparent in the whole cell lysate and mitochondrial fraction, we can draw no conclusion from this. There was no CTL1 detection in BMDMs with the method and antibody used for Figure 6. In the cells that were treated with LPS, there is marked increase in TOMM20, which is in keeping with the literature as LPS activation of macrophages has been previously shown to increase mitochondrial content in BMDMs and RAWs (Ji et al., 2021; Kasahara et al., 2011).

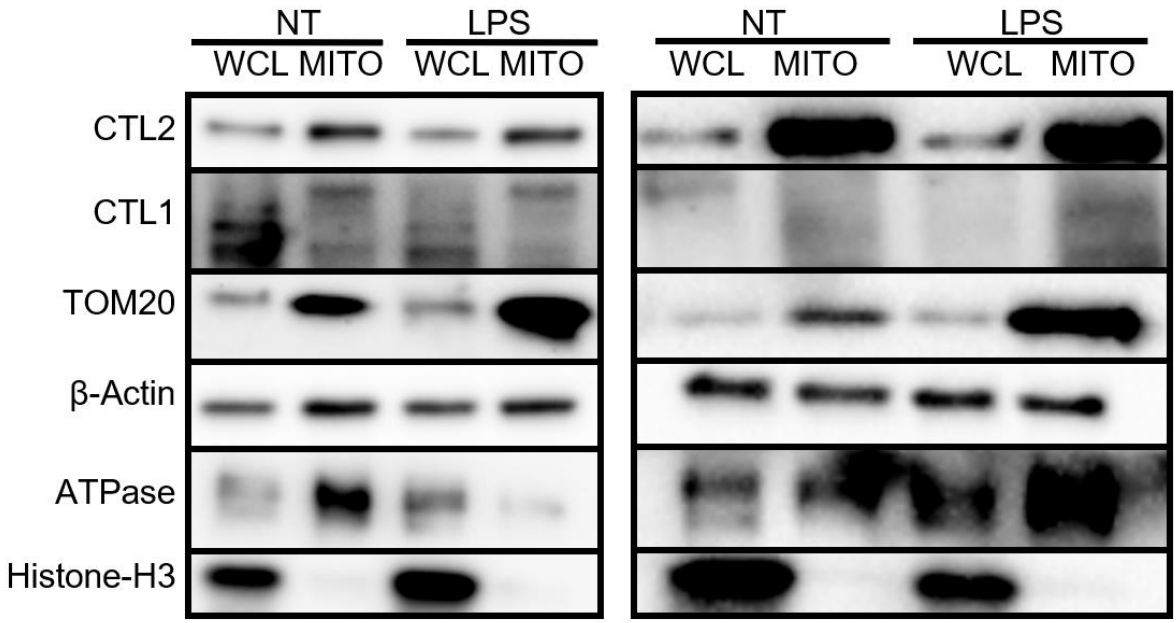
NT
LPS
NT
LPS
WCL MITO
WCL MITO
WCL MITO
WCL MITO
CTL2
CTL1
TOM20
β-Actin
ATPase
Histone-H3

Figure 5: Detection of CTL1/2 in mitochondrial enriched fraction. Samples are from approximately $2x10^8$ RAW 264.7s (P.17 and P.18) in denaturing buffer boiled at 95°C for 5 min. Samples were run on a precast 4-12% SDS gel at 120V for 132 min (left), 129 min (right). CTL1 (75 kDa), CTL2 (65 kDa), β-Actin (45 kDa), TOM20 (20kDa), and Histone3 (15kDa). Whole cell lysate (WCL) was removed prior to mitochondrial isolation version 2B. WCL and mitochondrial sample (MITO) were loaded with 5 µg of protein from pure Percoll gradient isolation. N=2, each replicate shown as individual panel.

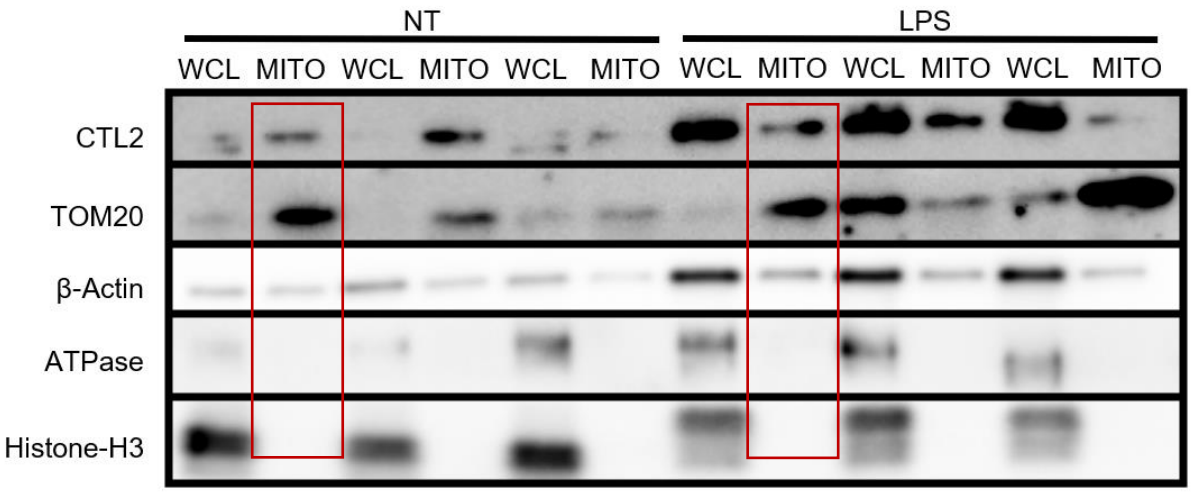
NT
LPS
WCL
MITO
WCL
MITO
WCL
MITO
WCL
MITO
WCL
MITO
WCL
MITO
CTL2
TOM20
β-Actin
ATPase
Histone-H3

Figure 6: Detection of CTL2 in mitochondrial enriched fraction. Samples are from a minimum of $5x10^7$ day 7 BMDMs treated with (right) or without (left) LPS in denaturing buffer boiled at 95℃ for 5 min. Samples were run on a precast 4-12% SDS gel at 120V for 125min. CTL2 (65 kDa), β-Actin (45 kDa), TOM20 (20kDa), and Histone3 (15kDa). Whole cell lysate (WCL) was removed prior to mitochondrial isolation. WCL and mitochondrial sample (MITO) were loaded with 5 µg of protein from pure Percoll gradient isolation using mitochondrial isolation version 2B. Samples were frozen prior to isolation. N=3, bone marrow from two mice per biological replicate pooled. Red boxed denote lanes of key interest.

6.2 Visualization of CTL transporters

To build on preliminary evidence from organelle fractionation and Western blotting, I next turned to microscopy to investigate potential interaction of CTL1/2 with the mitochondrial membrane. Given the rationale that mitochondrially-localized choline transporters have been identified in non-hepatic cells, I first aimed to validate that these transporters were present in primary hepatocytes. While the cells demonstrated typical binuclear morphology, stains for CTL1 and CTL2 did not reveal colocalization with mitochondria (Supplementary Figure 2).

Four CTL1 antibodies were tested to troubleshoot a protocol appropriate to detect CTL1 and CTL2 in macrophages. While CTL1 "C-term" antibody had been successfully used by others to stain CTL1 in various cells (Michel & Bakovic, 2009), improved visualization was observed with the CTL1 "C14" antibody, which was obtained commercially from Abcam. Therefore, this (CTL1-C14) antibody was used for most of the microscopy involving CTL1. A comparison between CTL1-C14 and C-term are noted in (Supplementary Figure 5). Since CTL1 is a validated plasma membrane protein, it was unexpected that staining highlighted a filament-like pattern in three separate cell types (BMDMs, RAW 264.7s, and C2C12s) (Figures 9-10 and Supplementary Figure 5).

To specifically test the main hypothesis of this project, I next determined the localization of CTL1 or CTL2 within macrophage cells. BMDMs and RAW 264.7s were treated ± LPS stimulation for 24 h before fixation and staining (Figure 7 and 8). Given previous reports, C2C12 cells were also used to identify a positive control (Supplementary Figure 5). In cells that were treated with LPS, there is no visual change to co-localization of CTL1 to MT detected in either BMDMs and RAW264.7s cells (Figures 9-10). In BMDMs, CTL2 co-localizes with mitochondria as seen in yellow in control and treated cells (Figure 7-F and I). In RAW 264.7s there appears to

be an increase in co-localization in LPS-treated cells compared to non-treated in Figure 8 (panels F and I).

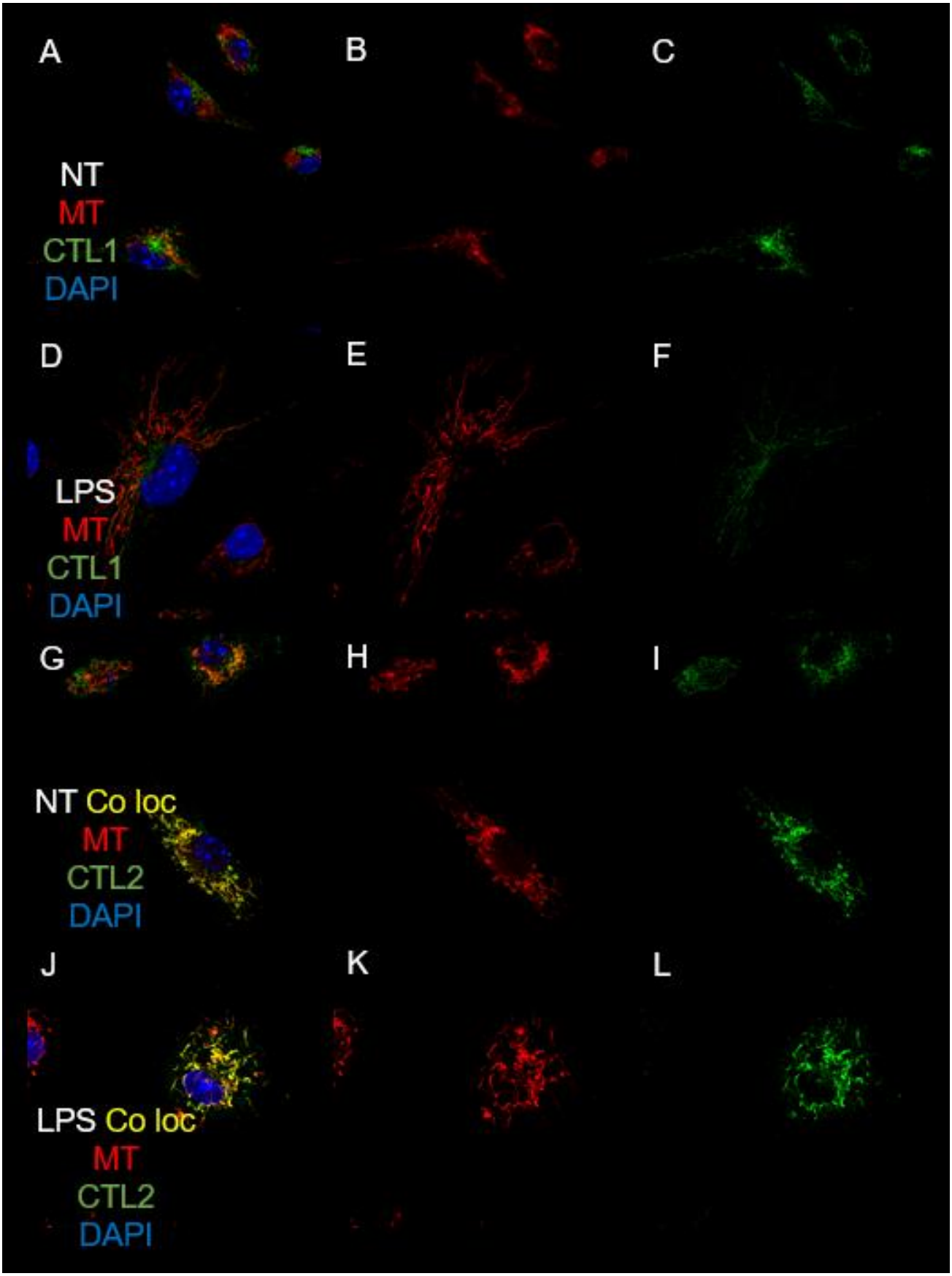
A
B
C
NT
MT
CTL1
DAPI
D
E
F
LPS
MT
CTL1
DAPI
G
H
I
NT Co loc
MT
CTL2
DAPI
J
K
L
LPS Co loc
MT
CTL2
DAPI

Figure 7: Detecting co-localization of BMDM mitochondria and CTL proteins. 55,000 WT BMDMs were plated on day 6 and received no treatment (NT) or 24 h LPS stimulation and were fixed at 37℃ with 4% PFA on day 7 using microscopy method 2. Images were captured on a Zeiss Axio-Observer.Z1-LSM 880-AiryScan confocal microscope on a chamber slide (1.5mm coverslip) 63x objective, using the AiryScan detector. CTL1/2 (Green: Oregon Green 488), MT (Red: MitoTracker™ CMXRos), and DAPI (Blue: nuclear stain). Red-green overlap shown in yellow. One image was taken for a single biological replicate. See Figure 9 for cell size.

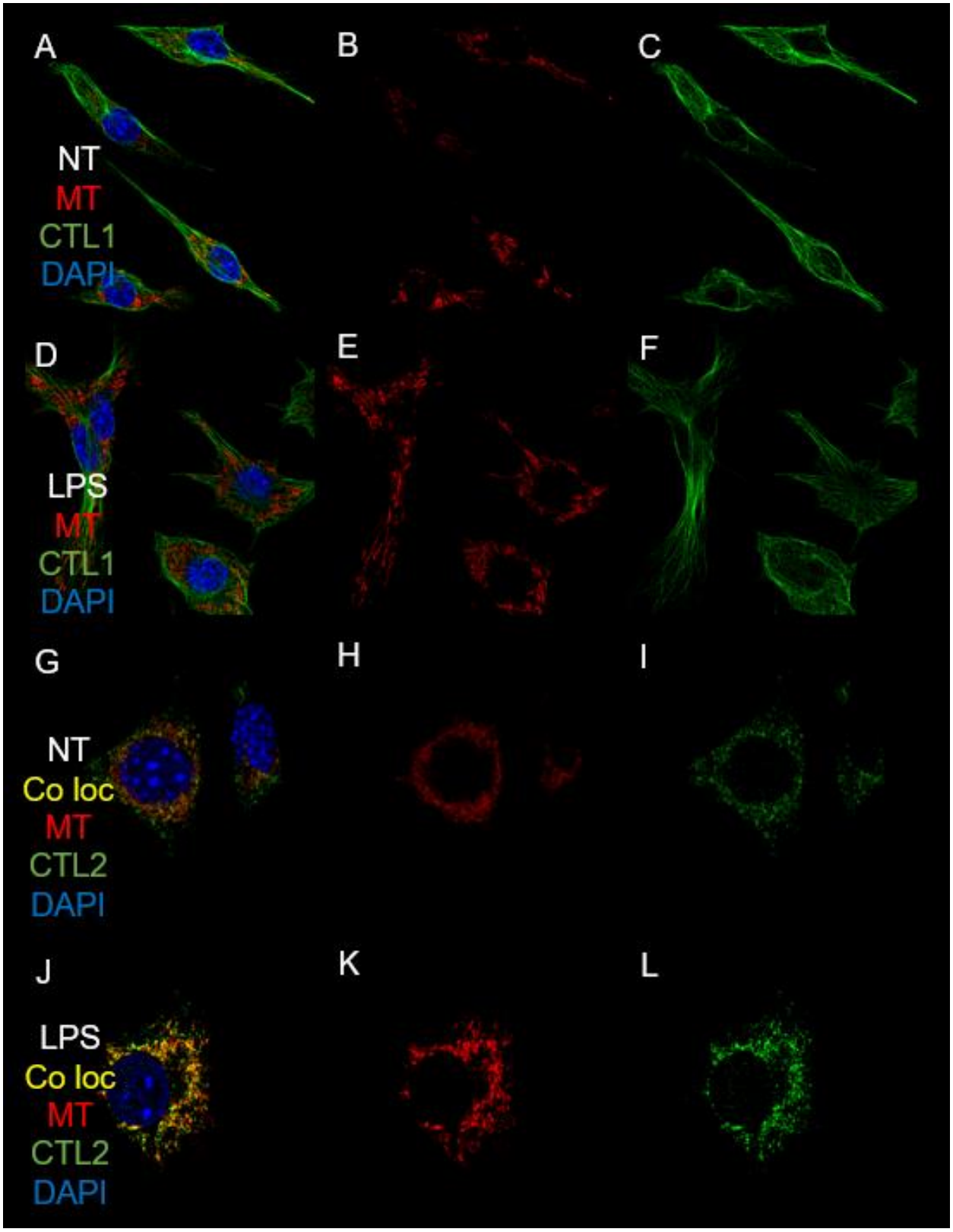
A
B
C
NT
MT
CTL1
DAPI
D
E
F
LPS
MT
CTL1
DAPI
G
H
I
NT
Co loc
MT
CTL2
DAPI
J
K
L
LPS
Co loc
MT
CTL2
DAPI

Figure 8: Detecting co-localization of RAW 264.7 mitochondria and CTL proteins. 15,000 RAWs P.20 no treatment (NT) or 24 h LPS stimulation and were fixed at 37℃ with 4% PFA on day 7, using microscopy method 2. Images were captured on a Zeiss Axio-Observer.Z1-LSM 880-AiryScan confocal microscope on a chamber slide (1.5mm coverslip) 63x objective, using the AiryScan detector. CTL1/2 (Green: Oregon Green 488), MT (Red: MitoTracker™ CMXRos), and DAPI (Blue: nuclear stain). Red-green overlap shown in yellow. One image was taken for a single biological replicate. See Figure 10 for cell size.

To further investigate if and how CTL1 and CTL2 interact with the mitochondrial membrane, high-resolution microscopy and computational analyses were used to confirm and quantify co-localization (Figure 9 and 10). Initially, widefield images were taken to develop microscopy staining and fixation protocols; however, the resolution this microscope provided was not high enough, nor were the images clear enough, even post deconvolution, to remove optical blur and non-specific fluorophore pixel assignment (Supplementary Figure 3). As such, final microscopy images were taken using super-resolution microscopy method AiryScan to better represent fluorophore location. These images were processed using a surface rendering program called Imaris 9.9.1, to quantify co-localization. Correction for background of AiryScan performed, resulting control stains images shown in Supplementary Figure 4. After using Imaris 9.9.1, it was revealed, that there is colocalization of both CTL1/2 and MT, in control and treated BMDMs and RAW 264.7s (middle panels, Figures 9 and 10, yellow). CTL1/2 proteins seem to interact in and around mitochondria and mitochondrial networks as shown in Figure 9-N and 10-N. Given the rapid division seen in RAW 264.7s, dividing cells were included in captured images for quantification of co-localization. These cells exhibit a high degree of co-localization (Figure 10-P).

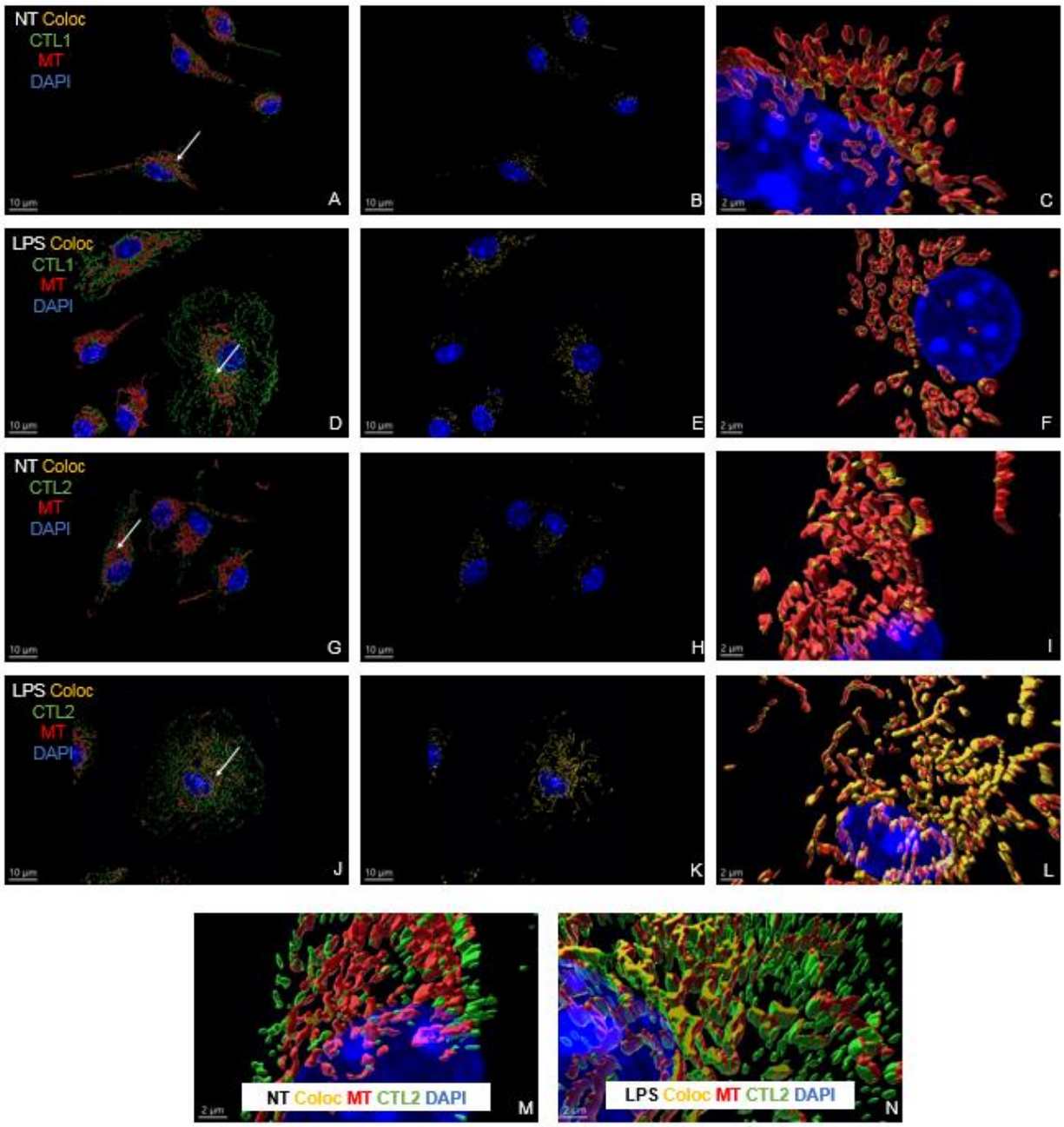
NT Coloc
CTL1
MT
DAPI
A
B
C
LPS Coloc
CTL1
MT
DAPI
D
E
F
NT Coloc
CTL2
MT
DAPI
G
H
I
LPS Coloc
CTL2
MT
DAPI
J
K
L
NT Coloc MT CTL2 DAPI
M
LPS Coloc MT CTL2 DAPI
N

Figure 9: 3D voxel visualization of BMDM CTL overlap with mitochondria. Images were captured as per Figure 9. Surface rendering was performed using Imaris 9.9.1 with Background subtraction LS, without smoothing, objects smaller than 30 voxels were filtered out. Object-Object statistics option, providing the volume of the overlapping voxels (yellow) between the mitochondria and the protein of interest (CTL1 or CTL2).

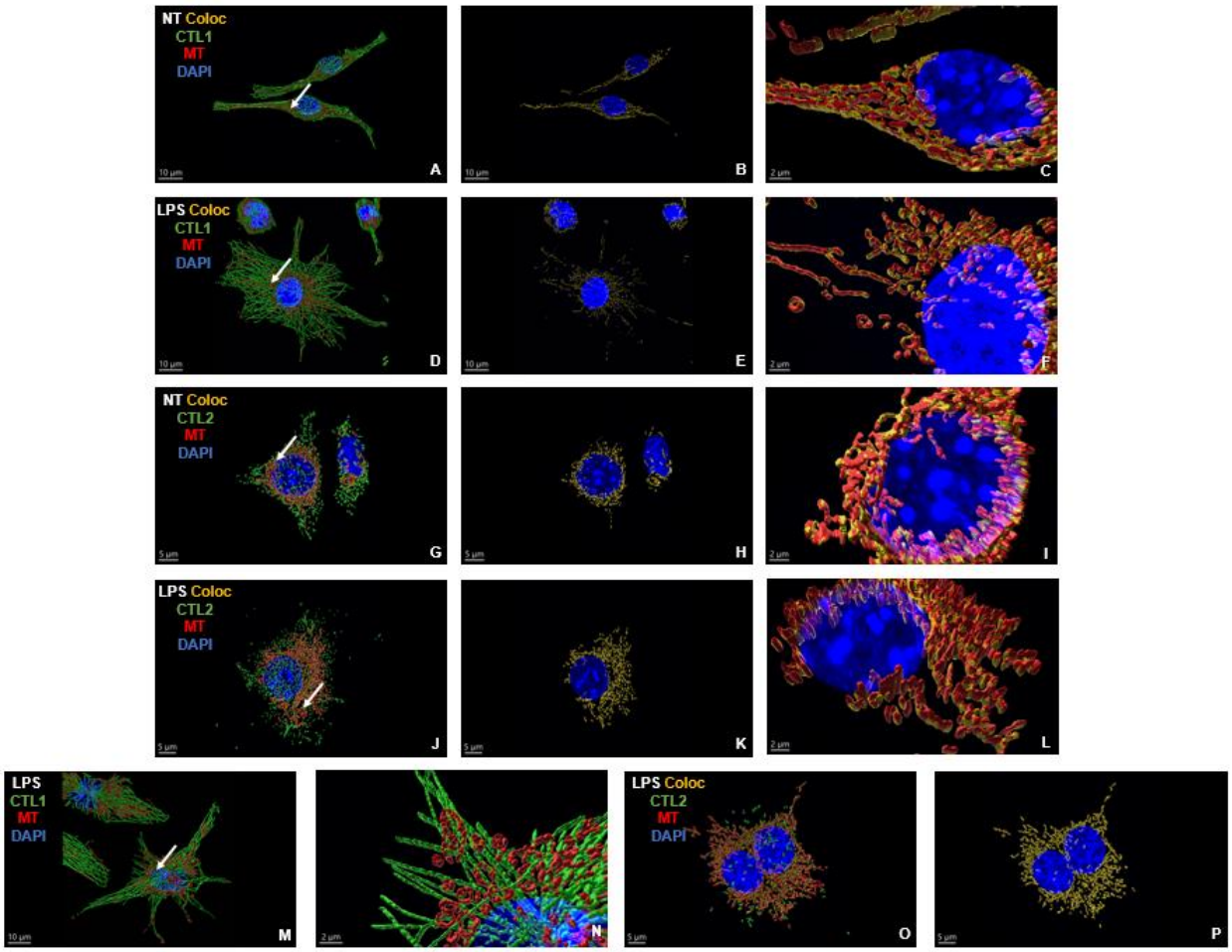
NT Coloc
CTL1
MT
DAPI
A
B
C
LPS Coloc
CTL1
MT
DAPI
D
E
F
NT Coloc
CTL2
MT
DAPI
G
H
I
LPS Coloc
CTL2
MT
DAPI
J
K
L
LPS
CTL1
MT
DAPI
M
N
LPS Coloc
CTL2
MT
DAPI
O
P

Figure 10: 3D voxel visualization of RAW 264.7 CTL overlap with mitochondria. Images were captured as per Figure 10. Surface rendering was performed using Imaris 9.9.1 with Background subtraction LS, without smoothing, objects smaller than 30 voxels were filtered out. Object-Object statistics option, providing the volume of the overlapping voxels (yellow) between the mitochondria and the protein of interest (CTL1 or CTL2).

Three-dimensional renderings of cells revealed volumes of mitochondria and CTL1/2. Where a fluorophore was detected from both proteins, created an overlapped (co-localization) volume (middle panels, Figure 9 and 10, yellow). The ratio between volume of co-localization compared to the volume of mitochondria was calculated, revealing an increase in CTL2 interaction with the mitochondria determined by co-localization in BMDMs treated with LPS (Figure 11-A). A similar level of CTL1/2 interaction was found in both untreated and treated RAW 264.7s (Figure 11-B).

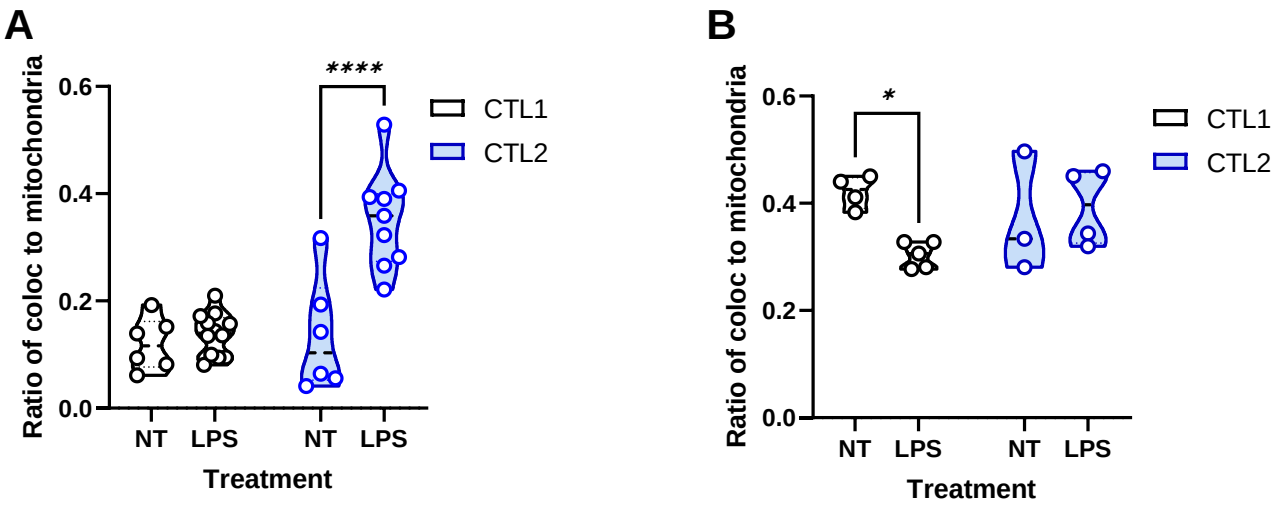
A
Ratio of coloc to mitochondria
0.6
0.4
0.2
0.0
****
NT
LPS
NT
LPS
Treatment
CTL1
CTL2
B
Ratio of coloc to mitochondria
0.6
0.4
0.2
0.0
*
NT
LPS
NT
LPS
Treatment
CTL1
CTL2

Figure 11: Quantification of volume of mitochondrial overlap of CTL proteins in macrophages. Data shown from Figure 9 BMDMs (A) and 10 RAW 264.7s (B). The ratio of overlapping colocalized voxels to the volume of mitochondria containing CTL signal shown. At least 3 frames of cells were taken for each stain and averaged. Statistical significance determined using Sidak's multiple comparisons from a two-way ANOVA (n=3-13 technical replicates per condition, * $p<0.05$, **** $p<0.0001$). Colocalization is the area where CTL and mitochondria overlap (coloc).

6.3 Determining if choline is taken up into isolated mitochondria

As the presence of CTL1/2 on the mitochondrial membrane indicated the potential for choline to be transported into the mitochondria of macrophages, the next step was to determine if this uptake could be detected and characterized. The Fullerton lab has previously performed choline uptake assay in BMDMs (Snider et al., 2018), but this has not been shown before in mitochondria isolated from macrophages. While whole cell uptake of choline, determined using tritiated choline (^{3}H-choline) in the presence of the inhibitors HC-3 and RSM-932a (an inhibitor of choline kinase) was re-validated (Figure 12-B), results for isolated mitochondria were variable, indicating the mitochondrial conditions may not have been ideal and required improvement. As noted in Figure 12, there was choline uptake into whole cells and mitochondria during a 30 min (A and B) or 5 min (C) uptake. While these data are displayed together, total DPM/mg values can not be compared between cells and mitochondria due to differences of cell to organelle surface area. These uptake assays were performed using crudely isolated mitochondria, maintained in a whole cell specific buffer with a simple uptake assay performed as an initial test (Figure 12-A and B). When crudely isolated mitochondria were tested in the presence of inhibitors (Figure 12-B), there was no inhibition of choline uptake, as would be expected if there was CTL1/2-mediated transport, as there was with the cells.

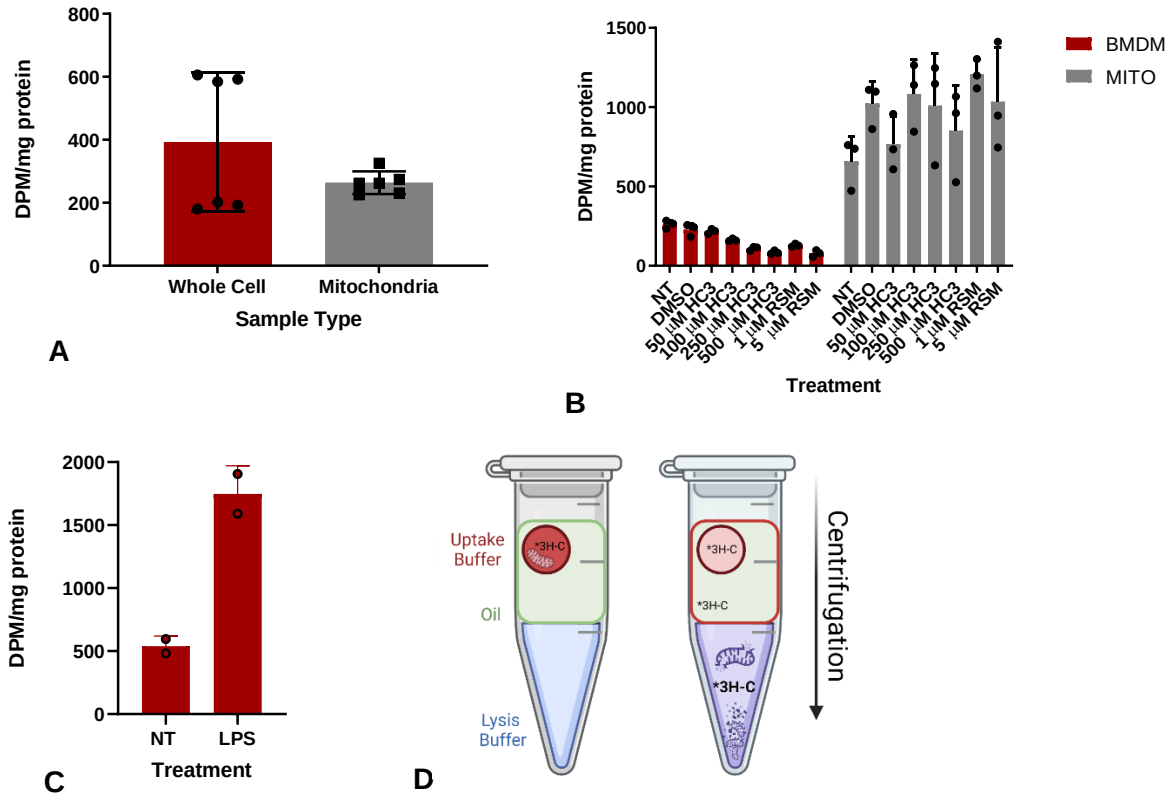
800
600
400
200
0
DPM/mg protein
Whole Cell
Mitochondria
Sample Type
A
1500
1000
500
0
DPM/mg protein
BMDM
MITO
NT
DMSO
50 µM HC3
100 µM HC3
250 µM HC3
500 µM HC3
1 µM RSM
5 µM RSM
Treatment
B
2000
1500
1000
500
0
DPM/mg protein
NT
LPS
Treatment
C
Uptake Buffer
Oil
Lysis Buffer
*3H-C
Centrifugation
D

Figure 12. LPS Challenged ^{3}H-choline uptake assays. DPM/µg of protein and measured by liquid scintillation. The mitochondria from approximately $1x10^{6}$ cells were used for each replicate. **(A)**Technical triplicate of WT BMDM and isolated mitochondria. Choline uptake was measured after 30 min at 37℃ of treatment with tritium labelled choline chloride. Mitochondrial uptake assays utilized simple suspension method. N=2 **(B)** Technical triplicate replicates of and N=1, were spiked with treatment in KRH as incubated for 25 min, allowing for a 5 min spin to remove the inhibitor. Cells were then incubated at 37℃ for 30 min with tritium-labelled choline chloride, after 24 h incubation. Mitochondrial uptake assays utilized simple suspension method **(C)** Technical duplicates of an N=1 from mitochondria crudely isolated from BMDM stimulated ± LPS for 24 h. Samples were acquired from oil layering assay. **(D)** Illustration of oil layering assay. Isolated mitochondria are spiked ^{3}H-choline in uptake buffer (red) which form a hydrophobic bubble in oil (green) on top of lysis buffer (blue). Following centrifugation, mitochondria migrate out of the bubble through the oil (washing step), removing external spiked ^{3}H-choline and lyse and pellet in the lysis buffer (purple).

As the protocol in Figure 12-A and B was not optimized for mitochondria and given the ability to maintain healthy mitochondria in suspension (approximately 1 h), a new approach was introduced. With the simple suspension uptake protocol, there was cause for concern with background contamination and continual uptake during pelleting steps. The new method of oil layering provided a method in which the microfuge tube has lysis buffer added first, followed by an oil layer and then assay buffer to provide an upper compartment for loading and uptake to occur. Following the uptake period, a brief centrifugation moves the mitochondria through the oil layer, effectively washing away excess ^{3}H-choline before entering the lysis buffer, which provides the organelle-specific ^{3}H-choline (Figure 12-D). This assay was performed in duplicate with a mitochondrial specific buffer, on mitochondria from at least 1 million cells (Figure 12-C). Cells were stimulated with LPS for 24 h before isolation. The new assays were performed for 5 min to provide a snapshot of uptake and to take into consideration the time restraint of isolating organelles. To confirm if mitochondria were intact post-isolation, a dye was used to determine the presence of active membrane potential of mitochondrial (data not shown), though further health assays may be warranted. Figure 12 shows that mitochondria isolated from macrophages uptake choline. However, these experiments need to be repeated to make a robust conclusion.

6.4 Choline incorporation into betaine

The observation that both CTL1/2 interact with the mitochondria and the preliminary finding that mitochondria uptake choline, I next sought to understand how. To determine if mitochondria oxidized choline into betaine, BMDMs were cultured under naïve conditions or with LPS for 24 h (Figure 13). These cells were then treated with ^{3}H-choline for 2, 4, 8 h. Metabolites from these cells were isolated and samples were run with TLC to detect PC, phosphocholine (Phos), free choline (Free), CDP-choline (CDP) and betaine (Figure 13-A). Samples were

visualized on the TLC plate using standard controls and radiation was determined with liquid scintillation. The incorporation of ^{3}H-choline into lipid and metabolite pools was shown relative to the amount of protein (Figure 13). The majority of labeled choline taken up was incorporated into PC (Figure 13-A) at the time points measured. The remaining four metabolites also showed a pattern of increasing incorporation over time. There were no differences between naïve and LPS-treated macrophages; however, more replicates are required to make conclusions. Importantly, this provides preliminary but novel evidence of choline conversion into betaine in macrophages. To build on these findings, cells were cultured for 8 and 24 h in the presence of ^{3}H-choline ± the choline uptake inhibitor HC-3 (Figure 13-B). While this data included four biological replicates, the variability of measured ^{3}H-betaine precluded robust conclusions. However, these data suggest that choline is converted to betaine in macrophages, and this may be sensitive to immune regulation.

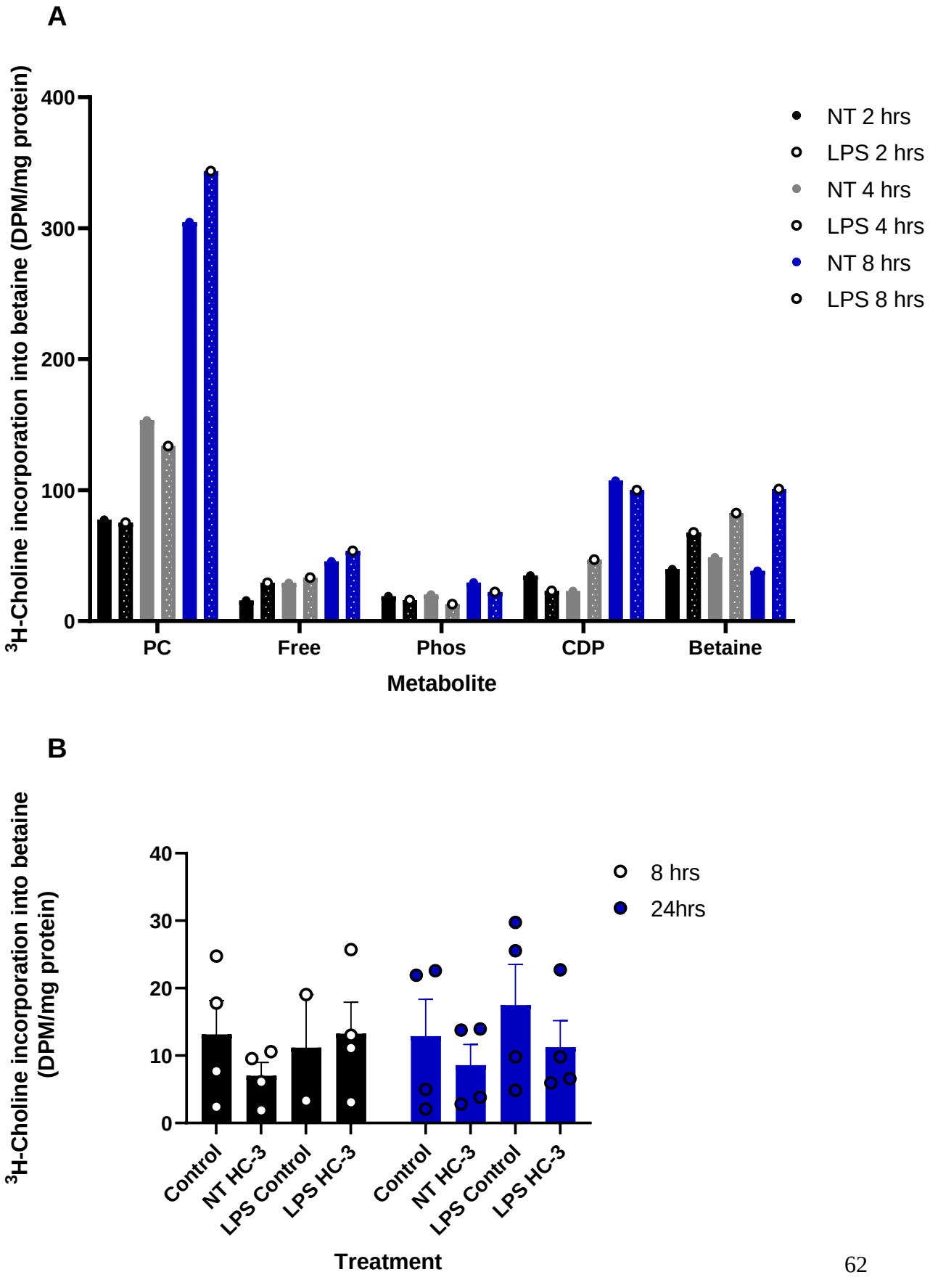
A
^{3}H-Choline incorporation into betaine (DPM/mg protein)
400
300
200
100
0
PC
Free
Phos
CDP
Betaine
Metabolite
NT 2 hrs
LPS 2 hrs
NT 4 hrs
LPS 4 hrs
NT 8 hrs
LPS 8 hrs
B
^{3}H-Choline incorporation into betaine (DPM/mg protein)
40
30
20
10
0
Control
NT HC-3
LPS Control
LPS HC-3
Control
NT HC-3
LPS Control
LPS HC-3
Treatment
8 hrs
24hrs

Figure 13: BMDM incorporation of ^{3}H-choline into choline metabolites overtime. DPM/ug of protein and measured by liquid scintillation. **(A)** Day 6 Naïve BMDMs were treated with ^{3}H-choline for 2, 4, and 8 h. A Bligh and Dyer was performed to extract lipid (PC) and aqueous (Free: free choline, Phos: phophocholine, CDP: CDP-choline and Betaine) metabolites. N=1 **(B)** Day 6 BMDMs were treated +/- LPS for 24 h, washed then treated +/- HC-3 [250 µM] and ^{3}H-choline for 8 and 24 h. A Bligh and Dyer was performed to extract aqueous metabolites, betaine standard used to isolate for betaine. N=4

6.5 Piloting metabolomics to characterize one carbon metabolism in macrophages

To continue to investigate the potential role(s) mitochondrial choline uptake may play in macrophage biology, I was assisted by the University of Ottawa Metabolomics Core Facility. In a pilot study, we sought to measure the levels of choline-related metabolites in BMDMs treated for 24 h with LPS, IL-4 or choline-free media. LPS and IL-4 provide two ends of macrophage polarization. While the immune profile of LPS and IL-4 stimulated macrophages is well characterized, how one carbon metabolites change under these conditions, remains unknown. These cells were pooled from two separate days and a panel of 20 metabolites involved in choline metabolism were reported in μM/million cells. Eight metabolites are reported in Table 1, to highlight choline metabolites relevant to the current project. Choline and betaine levels required a higher dilution given their apparent abundance and are not reported here. Though no conclusions can be drawn from such a simple pilot experiment, cells treated with LPS showed increased levels of 7 out of the 8 metabolites compared to naïve cells. These potential effects will be validated in future metabolomics experiments. Here, I show preliminary evidence that mitochondrial choline metabolism may play a role in macrophage biology.

Table 1: Metabolomics choline metabolites. Day 6 BMDMs were cultured with choline free media or HC-3 (250 μM), LPS (100 ng/ml), and IL-4 (20 ng/ml) for 24 h. Two separate experiments were performed on separate days and samples were pooled together for metabolic profiling with quantification using LC-MS. Metabolite concentration recorded as μM per million cells.

Metabolite	Treatment (µM/million cells)			
	NT	LPS	IL-4	Choline free
Betaine-aldehyde	$9.4x10^{-4}$	$1.2x10^{-3}$	$7.8\ x10^{-4}$	$7.8x10^{-4}$
Methionine	51.67	99.57	39.68	104.52
DMG	0.03	0.06	0.03	0.06
SAM	13.43	23.88	13.92	18.64
SAH	$6.7x10^{-3}$	$8.3\ x10^{-3}$	$9.7\ x10^{-3}$	$8.0\ x10^{-3}$
Folic acid	0.07	0.16	0.05	0.16
CDP-choline	0.05	0.03	0.04	0.07
PC	460.38	737.91	564.55	579.50

7.0 Discussion

While CTL1 has been identified to have a distinct role in macrophage immunometabolism (Snider et al., 2018), the role of CTL2 has yet to be identified. Research continues to allude to a relationship between the mechanism of choline oxidation and the activation of macrophages. I aimed to determine if choline transporters were present on the mitochondrial membrane of macrophages, whether choline uptake occurred, and how the choline incorporated through mitochondria was utilized by LPS activated macrophages.

7.1 CTL1 and CTL2 interact with the mitochondrial membrane of BMDMs

Building on the work done by Snider et al., 2018, I show evidence of CTL1 and CTL2 interacting with the mitochondria membrane in BMDMs and RAW 264.7s (Figure 9 and 10). While immunoblotting of CTL1 was inconclusive, CTL2 was found to be in mitochondrial enriched fractions (Figure 5 and 6). Snider et al 2018, confirmed that CTL1/2 but not organic cation transporters or the high-affinity choline transporter were present in macrophages. Interestingly, while the transcript expression of CTL2 increased with LPS stimulation, the total protein expression did not yield the same result (Snider et al., 2018). While CTL2 protein expression does not increase with LPS stimulation, I have shown that LPS stimulation increases the proportion of CTL2 interacting with the mitochondria compared to naïve treated cells, which showed a significant difference to naïve treatment (Figure 11-A). While IF staining was originally conducted to provide more support of CTL1/2 detection in the mitochondria, initial attempts to determine co-localization of CTL1/2 to the mitochondria proved to require higher resolution. Imaris 9.9.1. software did reveal that CTL1/2 interacts with the mitochondria and considering the level of volume of overlap, this is believed to be indicative of co-localization (Figure 9 and 10).

This data should be compared to cryo-immunogold electron microscopy (EM), which would allow for increased precision to determine co-localization (Wolff et al., 2014; Yi et al., 2015).

7.2 Mitochondrial choline uptake occurs in BMDMs

While choline transporters were detected in mitochondria, this does not prove that choline uptake can occur; therefore, I next assessed if functional choline uptake into mitochondria was occurring. While crudely isolating mitochondria to preform radiolabelled uptake assays has been done for several years, these studies use cellular systems involving high cell number (yeast) or highly metabolically active tissue (liver, kidney, and muscle), which provide robust mitochondrial biomass (O'Donoghue et al., 2009; Soetens et al., 1998). Several different approaches were taken to extract intact mitochondria from BMDMs. A dye was used to indicate membrane potential to determine levels of intact mitochondria post isolation, but mitochondrial protein output was limited. I have been able to show that choline uptake occurs in isolated mitochondria at 5 and 30 min assays (Figure 12-A-C).

7.3 Exploring the role of choline oxidation to betaine

For the first time, I have been able to show that not only does uptake of choline occur, but choline is metabolized to betaine and this process may increase in M(LPS) BMDMs (Figure 12). While the last incorporation study was not consistent, the data trends suggest that ^{3}H-choline can be converted to betaine. This experiment will need to be repeated with choline uptake inhibitors and LPS treatment to establish how incorporation is altered in activated macrophages when cells are deprived of choline.

In the presence of PC, macrophages produce IL-1β and ROS (Sanchez-Lopez et al., 2019; Xia et al., 2018). In the absence of PC, macrophages engage in mitophagy to prevent ROS

production. When this does not occur, metabolism of the cells shift to mediate cell damage by inducing mitophagy to prevent ROS (Sanchez-Lopez et al., 2019). Therefore, choline uptake helps maintain LPS activated macrophage mitochondria. LPS-stimulation induces a cell-damaging state that must be compensated by protective mechanisms to maintain cell integrity. Future research should evaluate the shift in cytokines and ROS species production shown to be influential when inhibiting choline metabolism. Mitochondrial fragmentation seems to be a compensatory, cell-protective mechanism occurring during macrophage activation, which protects damage to the mitochondria (Zezina et al., 2018). However, in the case of palmitate induced macrophages, the pro-inflammatory signals produced by the cell was hindered by fragmentation, in the case of lipo-toxicity, mitochondria undergo fragmentation to prevent an increase in inflammation (Samokhvalov et al., 2009). Without choline, macrophage mitochondria would sustain more damage and lead to immune dysfunction, which carries implications for immune-mediated diseases. Future research should explore the role of mitochondrial fragmentation in the context CTL2-mediated choline uptake.

Sanchez-Lopez et al., 2019 saw a similar affect of what happens when you increase betaine, when you inhibit choline uptake. This group determined that mitochondrial changes aggravated AMP-activated protein kinase (AMPK) to induce mitophagy and deactivate the NLRP3 inflammasome, which attenuated IL-1β levels (Sanchez-Lopez et al., 2019). Previously, work which had also explored choline's importance in macrophages was conducted by Snider et al., 2018. LPS treatment was shown to increase PC synthesis and choline uptake (Snider et al., 2018). Inhibition of choline uptake, affected LPS treated macrophages, causing an increase in TNFα and IL-6, and a decrease of IL-10. These effects were rescued in BMDMs treated with HC-3 when

provided excess choline. These findings indicate cell membrane localized CTL1 is responsible for choline uptake into macrophages.

Evidence for CTL2 mediated choline uptake into mitochondria is seen from Bennett et al., 2020. They showed that when comparing $CTL2^{-/-}$ platelets to CTL2 controls platelet, mitochondrial choline uptake and DMG levels are diminished, indicating a potential link to OCM. The authors emphasized that activated platelets require increased generation of ROS, mitochondrial oxygen consumption, and ATP production, which were hindered in $CTL2^{-/-}$ platelets. This evidence suggests that choline metabolism is a necessary part of platelet activation. They hypothesized, similar to my current study, that choline conversion to betaine is imperative, and that choline conversion to betaine is necessary for LPS-activated macrophages to generate ROS and ATP. Their metabolomics study also indicated a potential link to CTL2 mediated OCM.

7.5 Limitations of the study

Purity of sub cellular fractions is a known limitation of mitochondrial isolation. While gentler methods may be used for crude isolation, pure fractions are far harsher and generate a low proportion of mitochondrial output to cell input (Azimzadeh et al., 2016). The most successful run allowed for crude isolation where cell membrane, cytoskeletal proteins and nuclei were pelleted out at 1000 g (Appendix Figure 1). The method used to obtain this fraction in RAW 264.7s greatly reduces mitochondrial yield and therefore requires larger cell input than what can be provided from BMDMs from one mouse. While troubleshooting was performed in RAW 264.7s, the rapid cell proliferation of this cell line could mask biological relevance. THP-1s could provide another model of a human cell line of monocytes. While the AiryScan images captured in Figures 9 and 10 renders a relatively precise location of proteins, fluorophore signal from diffracted light provides limitations around a conclusion about transporter localization vs interaction.

Assessing uptake in isolated organelles requires high cell input and removes mitochondrial interaction with MAMs. While isolating mitochondria to determine if uptake is valid, this uptake occurs post stimulation only. Influencing mitochondrial uptake during ongoing stimulation should be considered. The simple suspension method provides a more rapid approach to determine if uptake occurs. Disadvantages of this method include: more disturbance of the mitochondria with washing and repeat pelleting, potential washing out of ^{3}H-choline, and continual metabolism of ^{3}H-choline during centrifugation with runs 2-5 min long. To control for these potential limitations, the experiments will need to include more controlled conditions. Samples kept at 4°C will slow metabolism, therefore samples should be maintained at 4°C following 22°C uptake. Background contamination remaining after washing during the simple suspension method can be determined with time zero trials. While choline transport might also be impacted by loss of membrane potential as this has not been assessed, including deactivated mitochondria would also serve as a no uptake control. Therefore, controls should include FCCP treated mitochondria to affect membrane potential) and snap freeze thawing (-80°C), where mitochondria are small enough to avoid lysis by ice crystals with intact structure but will become metabolically inactive/damaged. Health of the mitochondria following any damage from disturbance of resuspension and washing should be determined from using either the oil layer or simple suspension method. There is a limitation in determining how inhibiting mitochondrial choline uptake affects whole cell biology, as we are unable at present time to inhibit solely mitochondrial choline uptake *in vitro*. However, ^{3}H-Choline assay provided insight into choline uptake and metabolism outside of direct transport.

The oil layer method, while alleviates some of the above limitations, is challenging to prevent technical variation. Loading the sample into a hydrophobic oil bubble tends to result in multiple bubbles forming, and mitochondria being retained inside bubbles post centrifugation. This

results in an uneven amount of mitochondrial pelleting, which contributes to high technical variance. Future experiments should include transporter inhibition from WT BMDMs and isolated mitochondria from CTL1/2KO models. Acquiring these models would determine if mitochondrial choline transport is facilitated by CTL1/2, which are the only choline transporters known to exist in macrophages. Since we now know choline is up taken into the mitochondria and converted to betaine, something must facilitate transport, and if not CTL1/2, there could be another point of entry not yet identified.

7.4 Future directions

Inflammatory diseases are closely linked to the ability of the cell to produce lipids and maintain metabolism through osmolarity and one carbon metabolism. Choline uptake is central to these alterations, as shown in the body of evidence surrounding the relationship between choline-betaine and cancer cell metabolism (Du et al., 2017; Friso et al., 2017; Han et al., 2019). Future studies are needed to identify the precise mechanism crucial to these relationships as perturbing choline is related to disease. Epigenetic changes which result from histone modifications under the control of SAM should be evaluated in macrophages (Newman & Maddocks, 2017). Establishing how gene expression or histone methylation is affected when mitochondrial choline uptake is inhibited in M(LPS), would provide a logical next step for the current research. This may elucidate why CTL2 interaction with the mitochondria are increased in M(LPS) (Figure 11)

Altering human consumption of choline has been shown to influence the prognosis of cancer. Increasing choline consumption lowered the risk of colorectal cancer, while leukemia cells in adolescents were diminished through decreasing choline availability (Lu et al., 2015; Newman & Maddocks, 2017). These opposing demands of choline introduce potential avenues of drug

inhibition to treat cancer, but while denying cancer cells of one carbon metabolites to enable their proliferation would be advantageous, doing so risks the adverse effects of dampening OCM.

Further microscopy work assessing CTL1/2 localization in macrophages would benefit from an ER marker, as transporter localization to MAM contact sites and ER interaction are possible. Given how CTL1 in Figures 9-11 produce an uncharacteristic CTL1 stain, additional validation with CTL1KO fibroblasts and alternative co-localization to other cellular membranes should be preformed. It may be worthwhile to examine how limiting CTL1-mediated choline uptake through antibody blocking, or through CTLKOs, might change BMDM LPS-induced migration (Davidson & Wood, 2020). The current study would benefit from confirming findings with a second CTL2 antibody (Bennett et al., 2020; Ishikawa et al., 2020). Taken together, immunoblotting and IF indicate that mitochondrial choline transporters are present in macrophages. In addition to the continuation of work in macrophages, other immune cell types should be explored. Specifically, CTL1/2 gene expression has been found in B cells, T cells, and neutrophils, but not the proteins themselves (Karlsson et al., 2021; Thul et al., 2017).

Further assays will need to continue to explore how uptake is affected in mitochondria treated with inhibitors, antibodies or in CTL1/2 deficient cells. Specific inhibition of CTL2 would allow for cells to be permeabilized and block transport in vitro without removing the signals, contact sites and networks of mitochondria pertinent in whole cells verse fragmented isolated mitochondria. While the presence of ^{3}H-choline indicates that choline uptake into mitochondria still occurs after being isolated, isolated organelles may be more sensitive to inhibitor treatment (mitochondrial toxicity) and biological relevance may be masked.

All data to date indicate that indeed mitochondrial choline transport occurs in mitochondria and is converted to betaine, but what purpose this would have in macrophages and potential

relevance to activated macrophages remains unknown. While choline is oxidized to betaine in liver and kidney tissue to fuel OCM, betaine may play a role in controlling cellular stress after undergoing the metabolic changes required for activation. There is an established role of betaine as an osmolyte in RAW 264.7s and these cells do not process some OCM enzymes. Therefore betaine uptake may not be related to methyl donor requirements (Wettstein et al., 1998; Zhang et al., 1996). While not reported in this study, betaine was present in all cells at a level beyond the detectable range for the metabolomics pilot, indicating that betaine was present in large quantities of the cells. As such, this indicated that betaine is acquired externally from the cells and is not maintained from incorporation as stem cells.

Evaluating how reducing choline transport alters cellular biology continues to provide new insight into human disease. Fagerberg and colleagues characterized a neurodegenerative disease phenotype in human patients found to have homozygous frameshift mutations in the gene which codes for CTL1 (Fagerberg et al., 2020). In a fibroblast immortalized cell line developed from these patients, cells showed recovery of changes to organelles caused by the deletion of CTL1, when cells were treated with choline. How choline uptake could be recovered in $CTL1^{-/-}$ fibroblasts was answered by Taylor at al., 2021. The $CTL1^{-/-}$ fibroblasts were furthered revealed to have CTL2 on the plasma and mitochondrial membranes, allowing for compensation of choline uptake when CTL1 is not present (Taylor et al., 2021). Of note, CTL2 expression does not increase and therefore, cannot fully compensate for the loss of choline transport via CTL1, explaining why a disease phenotype would present itself when partial compensatory mechanisms are in place. Not only was CTL2 identified to uptake choline in these cells, but was revealed to be an ethanolamine transporter as well. (Taylor et al., 2021).

The current work aimed to further characterize the role of mitochondrial choline transporters in LPS stimulated macrophages. Repeating these assays in CTL1 or CTL2 deficient models would provide further insight into the potential role that the transporters play in mitochondrial choline uptake. This is body of preliminary work requiring more robust assessment of multiple biological replicates and more stringent treatments with immune challenge. Further work should explore other immune cells, cautious to the availability of limited cell number.

8.0 Conclusion

Choline is crucial to cell homeostasis. Understanding the metabolism of this molecule allows us to better understand and strengthen the link between metabolism and immunity. To identify if OCM plays a role in macrophages, this work presents evidence that CTL2 is the main choline transporter that interacts with the mitochondria and that this is increased when cells are polarized with LPS. Moreover, I also show preliminary evidence that there is functional choline uptake into the mitochondria and conversion to betaine. The immunometabolic significance of this process has yet to be determined; however, it may be that mitochondrial choline metabolism is a regulated process that may sustain specific macrophage programs, both in culture and *in vivo*.

9.0 References

Arumugam, M. K., Paal, M. C., Donohue, T. M., Ganesan, M., Osna, N. A., & Kharbanda, K. K. (2021). Beneficial Effects of Betaine: A Comprehensive Review. *Biology*, *10*(6), 456. https://doi.org/10.3390/biology10060456

Azimzadeh, P., Asadzadeh Aghdaei, H., Tarban, P., Akhondi, M. M., Shirazi, A., & Khorram Khorshid, H. R. (2016). Comparison of three methods for mitochondria isolation from the human liver cell line (HepG2). *Gastroenterology and Hepatology From Bed to Bench*, *9*(2), 105–113.

Bennett, J. A., Mastrangelo, M. A., Ture, S. K., Smith, C. O., Loelius, S. G., Berg, R. A., Shi, X., Burke, R. M., Spinelli, S. L., Cameron, S. J., Carey, T. E., Brookes, P. S., Gerszten, R. E., Sabater-Lleal, M., de Vries, P. S., Huffman, J. E., Smith, N. L., Morrell, C. N., & Lowenstein, C. J. (2020). The choline transporter Slc44a2 controls platelet activation and thrombosis by regulating mitochondrial function. *Nature Communications*, *11*. https://doi.org/10.1038/s41467-020-17254-w

Best, C. H., & Huntsman, M. E. (1935). The effect of choline on the liver fat of rats in various states of nutrition. *The Journal of Physiology*, *83*(3), 255–274.

Beyer, L. A., Galano, M. M., Nair, T. S., Kommareddi, P. K., Sha, S.-H., Raphael, Y., & Carey, T. E. (2011). Age-related changes in expression of CTL2/SLC44A2 and its isoforms in the mouse inner ear. *Hearing Research*, *282*(1), 63–68. https://doi.org/10.1016/j.heares.2011.09.004

Bianchi, M. E. (2007). DAMPs, PAMPs and alarmins: All we need to know about danger. *Journal of Leukocyte Biology*, *81*(1), 1–5. https://doi.org/10.1189/jlb.0306164

Brocker, C., Lassen, N., Estey, T., Pappa, A., Cantore, M., Orlova, V. V., Chavakis, T., Kavanagh, K. L., Oppermann, U., & Vasiliou, V. (2010). Aldehyde dehydrogenase 7A1 (ALDH7A1) is a novel enzyme involved in cellular defense against hyperosmotic stress. *The Journal of Biological Chemistry*, *285*(24), 18452–18463. https://doi.org/10.1074/jbc.M109.077925

Chinnery, P. F., & Schon, E. A. (2003). Mitochondria. *Journal of Neurology, Neurosurgery & Psychiatry*, *74*(9), 1188–1199. https://doi.org/10.1136/jnnp.74.9.1188

Corbin, K. D., & Zeisel, S. H. (2012). Choline metabolism provides novel insights into nonalcoholic fatty liver disease and its progression. *Current Opinion in Gastroenterology*, *28*(2), 159–165. https://doi.org/10.1097/MOG.0b013e32834e7b4b

Correia, I., Chu, D., Chou, Y.-H., Goldman, R. D., & Matsudaira, P. (1999). Integrating the Actin and Vimentin Cytoskeletons: Adhesion-dependent Formation of Fimbrin–Vimentin Complexes in Macrophages. *The Journal of Cell Biology*, *146*, 12.

Cuillerier, A., Ruiz, M., Daneault, C., Forest, A., Rossi, J., Vasam, G., Cairns, G., Cadete, V., Des Rosiers, C., & Burelle, Y. (2021). Adaptive optimization of the OXPHOS assembly line partially compensates lrpprc-dependent mitochondrial translation defects in mice. *Communications Biology*, *4*, 989. https://doi.org/10.1038/s42003-021-02492-5

Davidson, A. J., & Wood, W. (2020). Macrophages Use Distinct Actin Regulators to Switch Engulfment Strategies and Ensure Phagocytic Plasticity In Vivo. *Cell Reports*, *31*(8), 107692. https://doi.org/10.1016/j.celrep.2020.107692

Du, Y.-F., Lin, F.-Y., Long, W.-Q., Luo, W.-P., Yan, B., Xu, M., Mo, X.-F., & Zhang, C.-X. (2017). Serum betaine but not choline is inversely associated with breast cancer risk: A case–control study in China. *European Journal of Nutrition*, *56*(3), 1329–1337. https://doi.org/10.1007/s00394-016-1183-3

Fagerberg, C. R., Taylor, A., Distelmaier, F., Schrøder, H. D., Kibæk, M., Wieczorek, D., Tarnopolsky, M., Brady, L., Larsen, M. J., Jamra, R. A., Seibt, A., Hejbøl, E. K., Gade, E., Markovic, L., Klee, D., Nagy, P., Rouse, N., Agarwal, P., Dolinsky, V. W., & Bakovic, M. (2020). Choline transporter-like 1 deficiency causes a new type of childhood-onset neurodegeneration. *Brain*, *143*(1), 94–111. https://doi.org/10.1093/brain/awz376

Fagone, P., & Jackowski, S. (2013). Phosphatidylcholine and the CDP-choline cycle. *Biochimica Et Biophysica Acta*, *1831*(3), 523–532. https://doi.org/10.1016/j.bbalip.2012.09.009

Friso, S., Udali, S., De Santis, D., & Choi, S.-W. (2017). One-carbon metabolism and epigenetics. *Molecular Aspects of Medicine*, *54*, 28–36. https://doi.org/10.1016/j.mam.2016.11.007

Ghoshal, A. K., Ahluwalia, M., & Farber, E. (1983). The rapid induction of liver cell death in rats fed a choline-deficient methionine-low diet. *The American Journal of Pathology*, *113*(3), 309–314.

Gibellini, F., & Smith, T. K. (2010). The Kennedy pathway—De novo synthesis of phosphatidylethanolamine and phosphatidylcholine. *IUBMB Life*, *62*(6), 414–428. https://doi.org/10.1002/iub.337

Goerdt, S., Politz, O., Schledzewski, K., Birk, R., & al, et. (1999). Alternative versus classical activation of Macrophages. *Pathobiology*, *67*(5/6), 222–226.

Grossman, E. B., & Hebert, S. C. (1989). Renal inner medullary choline dehydrogenase activity: Characterization and modulation. *American Journal of Physiology-Renal Physiology*, *256*(1), F107–F112. https://doi.org/10.1152/ajprenal.1989.256.1.F107

Han, P., Bidulescu, A., Barber, J. R., Zeisel, S. H., Joshu, C. E., Prizment, A., Vitolins, M. Z., & Platz, E. A. (2019). Dietary choline and betaine intakes and risk of total and lethal prostate

cancer in the Atherosclerosis Risk in Communities (ARIC) Study. *Cancer Causes & Control : CCC*, *30*(4), 343–354. https://doi.org/10.1007/s10552-019-01148-4

Hartroft, W. S., Ridout, J. H., Sellers, E. A., & Best, C. H. (1952). Atheromatous changes in aorta, carotid and coronary arteries of choline-deficient rats. *Proceedings of the Society for Experimental Biology and Medicine. Society for Experimental Biology and Medicine (New York, N.Y.)*, *81*(2), 384–393. https://doi.org/10.3181/00379727-81-19885

Haubrich, D. R., & Gerber, N. H. (1981). Choline dehydrogenase: Assay, properties and inhibitors. *Biochemical Pharmacology*, *30*(21), 2993–3000. https://doi.org/10.1016/0006-2952(81)90265-3

Hoppins, S., Lackner, L., & Nunnari, J. (2007). The Machines that Divide and Fuse Mitochondria. *Annual Review of Biochemistry*, *76*(1), 751–780. https://doi.org/10.1146/annurev.biochem.76.071905.090048

Horner, S. M., Liu, H. M., Park, H. S., Briley, J., & Gale, M. (2011). Mitochondrial-associated endoplasmic reticulum membranes (MAM) form innate immune synapses and are targeted by hepatitis C virus. *Proceedings of the National Academy of Sciences of the United States of America*, *108*(35), 14590–14595. https://doi.org/10.1073/pnas.1110133108

Ishikawa, T., Suwanai, H., Shikuma, J., Suzuki, R., Yamanaka, T., Odawara, M., & Inazu, M. (2020). Protein kinase C promotes choline transporter-like protein 1 function via improved cell surface expression in immortalized human hepatic cells. *Molecular Medicine Reports*, *21*(2), 777–785. https://doi.org/10.3892/mmr.2019.10894

Jacob, R. A., Jenden, D. J., Allman-Farinelli, M. A., & Swendseid, M. E. (1999). Folate nutriture alters choline status of women and men fed low choline diets. *The Journal of Nutrition*, *129*(3), 712–717. https://doi.org/10.1093/jn/129.3.712

Ji, S. Y., Cha, H.-J., Molagoda, I. M. N., Kim, M. Y., Kim, S. Y., Hwangbo, H., Lee, H., Kim, G.-Y., Kim, D.-H., Hyun, J. W., Kim, H.-S., Kim, S., Jin, C.-Y., & Choi, Y. H. (2021). Suppression of Lipopolysaccharide-Induced Inflammatory and Oxidative Response by 5-Aminolevulinic Acid in RAW 264.7 Macrophages and Zebrafish Larvae. *Biomolecules & Therapeutics*, *29*(6), 685–696. https://doi.org/10.4062/biomolther.2021.030

Jukes, T. H. (1940). Effect of Choline and Other Supplements on Perosis: Two Figures. *The Journal of Nutrition*, *20*(5), 445–458. https://doi.org/10.1093/jn/22.5.445

Kapetanovic, R., Afroz, S. F., Ramnath, D., Lawrence, G. M., Okada, T., Curson, J. E., de Bruin, J., Fairlie, D. P., Schroder, K., St John, J. C., Blumenthal, A., & Sweet, M. J. (2020). Lipopolysaccharide promotes Drp1-dependent mitochondrial fission and associated inflammatory responses in macrophages. *Immunology and Cell Biology*, *98*(7), 528–539. https://doi.org/10.1111/imcb.12363

Kaplan, C. P., Porter, R. K., & Brand, M. D. (1993). The choline transporter is the major site of control of choline oxidation in isolated rat liver mitochondria. *FEBS Letters*, *321*(1), 24–26. https://doi.org/10.1016/0014-5793(93)80613-y

Karlsson, M., Zhang, C., Méar, L., Zhong, W., Digre, A., Katona, B., Sjöstedt, E., Butler, L., Odeberg, J., Dusart, P., Edfors, F., Oksvold, P., von Feilitzen, K., Zwahlen, M., Arif, M., Altay, O., Li, X., Ozcan, M., Mardinoglu, A., … Lindskog, C. (2021). A single-cell type transcriptomics map of human tissues. *Science Advances*, *7*(31), eabh2169. https://doi.org/10.1126/sciadv.abh2169

Kasahara, E., Sekiyama, A., Hori, M., Hara, K., Takahashi, N., Konishi, M., Sato, E. F., Matsumoto, S., Okamura, H., & Inoue, M. (2011). Mitochondrial density contributes to the

immune response of macrophages to lipopolysaccharide via the MAPK pathway. *FEBS Letters*, *585*(14), 2263–2268. https://doi.org/10.1016/j.febslet.2011.05.049

Kennedy, E. P., & Weiss, S. B. (1956). The function of cytidine coenzymes in the biosynthesis of phospholipides. *The Journal of Biological Chemistry*, *222*(1), 193–214.

Kent, C. (1997). CTP:phosphocholine cytidylyltransferase. *Biochimica et Biophysica Acta (BBA) - Lipids and Lipid Metabolism*, *1348*(1), 79–90. https://doi.org/10.1016/S0005-2760(97)00112-4

Kommareddi, P. K., Nair, T. S., Raphael, Y., Telian, S. A., Kim, A. H., Arts, H. A., El-Kashlan, H. K., & Carey, T. E. (2007). Cochlin Isoforms and Their Interaction with CTL2 (SLC44A2) in the Inner Ear. *Journal of the Association for Research in Otolaryngology*, *8*(4), 435–446. https://doi.org/10.1007/s10162-007-0099-2

Kommareddi, P. K., Nair, T. S., Thang, L. V., Galano, M. M., Babu, E., Ganapathy, V., Kanazawa, T., McHugh, J. B., & Carey, T. E. (2010). Isoforms, Expression, Glycosylation, and Tissue Distribution of CTL2/SLC44A2. *The Protein Journal*, *29*(6), 417–426. https://doi.org/10.1007/s10930-010-9268-y

Ley, K., Laudanna, C., Cybulsky, M. I., & Nourshargh, S. (2007). Getting to the site of inflammation: The leukocyte adhesion cascade updated. *Nature Reviews Immunology*, *7*(9), Article 9. https://doi.org/10.1038/nri2156

Lin, C.-S., & Wu, R.-D. (1986). Choline oxidation and choline dehydrogenase. *Journal of Protein Chemistry*, *5*(3), 193–200. https://doi.org/10.1007/BF01025488

Lockman, P. R., & Allen, D. D. (2002). The transport of choline. *Drug Development and Industrial Pharmacy*, *28*(7), 749–771. https://doi.org/10.1081/ddc-120005622

Lu, M.-S., Fang, Y.-J., Pan, Z.-Z., Zhong, X., Zheng, M.-C., Chen, Y.-M., & Zhang, C.-X. (2015). Choline and Betaine Intake and Colorectal Cancer Risk in Chinese Population: A Case-Control Study. *PLOS ONE*, *10*(3), e0118661. https://doi.org/10.1371/journal.pone.0118661

Martinez, F. O. (2011). Regulators of macrophage activation. *European Journal of Immunology*, *41*(6), 1531–1534. https://doi.org/10.1002/eji.201141670

McMurray, W. C., & Magee, W. L. (1972). Phospholipid metabolism. *Annual Review of Biochemistry*, *41*(10), 129–160. https://doi.org/10.1146/annurev.bi.41.070172.001021

Meng, F., & Lowell, C. A. (1997). Lipopolysaccharide (LPS)-induced Macrophage Activation and Signal Transduction in the Absence of Src-Family Kinases Hck, Fgr, and Lyn. *The Journal of Experimental Medicine*, *185*(9), 1661–1670.

Menzies, C., Naz, S., Patten, D., Alquier, T., Bennett, B. M., & Lacoste, B. (2021). Distinct Basal Metabolism in Three Mouse Models of Neurodevelopmental Disorders. *ENeuro*, *8*(2). https://doi.org/10.1523/ENEURO.0292-20.2021

Michel, V., & Bakovic, M. (2009). The solute carrier 44A1 is a mitochondrial protein and mediates choline transport. *FASEB Journal: Official Publication of the Federation of American Societies for Experimental Biology*, *23*(8), 2749–2758. https://doi.org/10.1096/fj.08-121491

Michel, V., Yuan, Z., Ramsubir, S., & Bakovic, M. (2006). Choline transport for phospholipid synthesis. *Experimental Biology and Medicine (Maywood, N.J.)*, *231*(5), 490–504. https://doi.org/10.1177/153537020623100503

Mosser, D. M., & Edwards, J. P. (2008). Exploring the full spectrum of macrophage activation. *Nature Reviews. Immunology*, *8*(12), 958–969. https://doi.org/10.1038/nri2448

Nair, T. S., Kozma, K. E., Hoefling, N. L., Kommareddi, P. K., Ueda, Y., Gong, T.-W., Lomax, M. I., Lansford, C. D., Telian, S. A., Satar, B., Arts, H. A., El-Kashlan, H. K., Berryhill, W. E., Raphael, Y., & Carey, T. E. (2004). Identification and Characterization of Choline Transporter-Like Protein 2, an Inner Ear Glycoprotein of 68 and 72 kDa That Is the Target of Antibody-Induced Hearing Loss. *The Journal of Neuroscience*, *24*(7), 1772–1779. https://doi.org/10.1523/JNEUROSCI.5063-03.2004

Newman, A. C., & Maddocks, O. D. K. (2017). One-carbon metabolism in cancer. *British Journal of Cancer*, *116*(12), Article 12. https://doi.org/10.1038/bjc.2017.118

Niculescu, M. D., & Zeisel, S. H. (2002). Diet, Methyl Donors and DNA Methylation: Interactions between Dietary Folate, Methionine and Choline. *The Journal of Nutrition*, *132*(8), 2333S-2335S. https://doi.org/10.1093/jn/132.8.2333S

Obeid, R. (2013). The Metabolic Burden of Methyl Donor Deficiency with Focus on the Betaine Homocysteine Methyltransferase Pathway. *Nutrients*, *5*(9), Article 9. https://doi.org/10.3390/nu5093481

O'Donoghue, N., Sweeney, T., Donagh, R., Clarke, K. J., & Porter, R. K. (2009). Control of choline oxidation in rat kidney mitochondria. *Biochimica et Biophysica Acta (BBA) - Bioenergetics*, *1787*(9), 1135–1139. https://doi.org/10.1016/j.bbabio.2009.04.014

O'Regan, S., Traiffort, E., Ruat, M., Cha, N., Compaore, D., & Meunier, F. M. (2000). An electric lobe suppressor for a yeast choline transport mutation belongs to a new family of transporter-like proteins. *Proceedings of the National Academy of Sciences of the United States of America*, *97*(4), 1835–1840. https://doi.org/10.1073/pnas.030339697

Pietruszko, R., & Chern, M.-K. (2001). Betaine aldehyde dehydrogenase from rat liver mitochondrial matrix. *Chemico-Biological Interactions*, *130–132*, 193–199. https://doi.org/10.1016/S0009-2797(00)00277-5

Salmon, W. D., & Copeland, D. H. (1954). Liver carcinoma and related lesions in chronic choline deficiency. *Annals of the New York Academy of Sciences*, *57*(6), 665–677. https://doi.org/10.1111/j.1749-6632.1954.tb36443.x

Samokhvalov, V., Bilan, P. J., Schertzer, J. D., Antonescu, C. N., & Klip, A. (2009). Palmitate- and lipopolysaccharide-activated macrophages evoke contrasting insulin responses in muscle cells. *American Journal of Physiology-Endocrinology and Metabolism*, *296*(1), E37–E46. https://doi.org/10.1152/ajpendo.90667.2008

Sanchez-Lopez, E., Zhong, Z., Stubelius, A., Sweeney, S. R., Booshehri, L. M., Antonucci, L., Liu-Bryan, R., Lodi, A., Terkeltaub, R., Lacal, J. C., Murphy, A. N., Hoffman, H. M., Tiziani, S., Guma, M., & Karin, M. (2019). Choline Uptake and Metabolism Modulate Macrophage IL-1β and IL-18 Production. *Cell Metabolism*, *29*(6), 1350-1362.e7. https://doi.org/10.1016/j.cmet.2019.03.011

Sanders, L. M., & Zeisel, S. H. (2007). Choline. *Nutrition Today*, *42*(4), 181–186. https://doi.org/10.1097/01.NT.0000286155.55343.fa

Schmidt, O., Pfanner, N., & Meisinger, C. (2010). Mitochondrial protein import: From proteomics to functional mechanisms. *Nature Reviews Molecular Cell Biology*, *11*(9), Article 9. https://doi.org/10.1038/nrm2959

Snider, S. A., Margison, K. D., Ghorbani, P., LeBlond, N. D., O'Dwyer, C., Nunes, J. R. C., Nguyen, T., Xu, H., Bennett, S. A. L., & Fullerton, M. D. (2018). Choline transport links

macrophage phospholipid metabolism and inflammation. *The Journal of Biological Chemistry*, *293*(29), 11600–11611. https://doi.org/10.1074/jbc.RA118.003180

Soetens, O., Crabeel, M., El Moualij, B., Duyckaerts, C., & Sluse, F. (1998). Transport of arginine and ornithine into isolated mitochondria of Saccharomyces cerevisiae. *European Journal of Biochemistry*, *258*(2), 702–709. https://doi.org/10.1046/j.1432-1327.1998.2580702.x

Solé-Navais, P., Cavallé-Busquets, P., Fernandez-Ballart, J. D., & Murphy, M. M. (2016). Early pregnancy B vitamin status, one carbon metabolism, pregnancy outcome and child development. *Biochimie*, *126*, 91–96. https://doi.org/10.1016/j.biochi.2015.12.003

Stead, L. M., Brosnan, J. T., Brosnan, M. E., Vance, D. E., & Jacobs, R. L. (2006). Is it time to reevaluate methyl balance in humans? *The American Journal of Clinical Nutrition*, *83*(1), 5–10. https://doi.org/10.1093/ajcn/83.1.5

Taanman, J.-W. (1999). The mitochondrial genome: Structure, transcription, translation and replication. *Biochimica et Biophysica Acta (BBA) - Bioenergetics*, *1410*(2), 103–123. https://doi.org/10.1016/S0005-2728(98)00161-3

Taylor, A., Grapentine, S., Ichhpuniani, J., & Bakovic, M. (2021). Choline transporter-like proteins 1 and 2 are newly identified plasma membrane and mitochondrial ethanolamine transporters. *Journal of Biological Chemistry*, *296*, 100604. https://doi.org/10.1016/j.jbc.2021.100604

Thul, P. J., Åkesson, L., Wiking, M., Mahdessian, D., Geladaki, A., Ait Blal, H., Alm, T., Asplund, A., Björk, L., Breckels, L. M., Bäckström, A., Danielsson, F., Fagerberg, L., Fall, J., Gatto, L., Gnann, C., Hober, S., Hjelmare, M., Johansson, F., … Lundberg, E. (2017). A subcellular map of the human proteome. *Science (New York, N.Y.)*, *356*(6340), eaal3321. https://doi.org/10.1126/science.aal3321

Traiffort, E., O'Regan, S., & Ruat, M. (2013). The choline transporter-like family SLC44: Properties and roles in human diseases. *Molecular Aspects of Medicine*, *34*(2–3), 646–654. https://doi.org/10.1016/j.mam.2012.10.011

Tucek, S. (1985). Regulation of acetylcholine synthesis in the brain. *Journal of Neurochemistry*, *44*(1), 11–24. https://doi.org/10.1111/j.1471-4159.1985.tb07106.x

Ueland, P. M., Holm, P. I., & Hustad, S. (2005). Betaine: A key modulator of one-carbon metabolism and homocysteine status. *Clinical Chemistry and Laboratory Medicine (CCLM)*, *43*(10), 1069–1075. https://doi.org/10.1515/CCLM.2005.187

Vance, D. E., & Vance, J. E. (2009). Physiological consequences of disruption of mammalian phospholipid biosynthetic genes. *Journal of Lipid Research*, *50 Suppl*, S132-137. https://doi.org/10.1194/jlr.R800048-JLR200

Veskovic, M., Mladenovic, D., Milenkovic, M., Tosic, J., Borozan, S., Gopcevic, K., Labudovic-Borovic, M., Dragutinovic, V., Vucevic, D., Jorgacevic, B., Isakovic, A., Trajkovic, V., & Radosavljevic, T. (2019). Betaine modulates oxidative stress, inflammation, apoptosis, autophagy, and Akt/mTOR signaling in methionine-choline deficiency-induced fatty liver disease. *European Journal of Pharmacology*, *848*, 39–48. https://doi.org/10.1016/j.ejphar.2019.01.043

Waite, K. A., Cabilio, N. R., & Vance, D. E. (2002). Choline Deficiency–Induced Liver Damage Is Reversible in Pemt−/− Mice. *The Journal of Nutrition*, *132*(1), 68–71. https://doi.org/10.1093/jn/132.1.68

Wang, X., & Schwarz, T. L. (2009). The Mechanism of Ca2+-Dependent Regulation of Kinesin-Mediated Mitochondrial Motility. *Cell*, *136*(1), 163–174. https://doi.org/10.1016/j.cell.2008.11.046

Warskulat, U., Wettstein, M., & Häussinger, D. (1995). Betaine is an osmolyte in RAW 264.7 mouse macrophages. *FEBS Letters*, *377*(1), 47–50. https://doi.org/10.1016/0014-5793(95)01317-2

Wettstein, M., Weik, C., Holneicher, C., & Häussinger, D. (1998). Betaine as an osmolyte in rat liver: Metabolism and cell-to-cell interactions. *Hepatology*, *27*(3), 787–793. https://doi.org/10.1002/hep.510270321

Willoughby, M. L., & Jewell, F. J. (1966). Investigation of folic acid requirements in pregnancy. *British Medical Journal*, *2*(5529), 1568–1571.

Wirtz, K. W. (1997). Phospholipid transfer proteins revisited. *Biochemical Journal*, *324*(Pt 2), 353–360.

Wolff, N. A., Ghio, A. J., Garrick, L. M., Garrick, M. D., Zhao, L., Fenton, R. A., & Thévenod, F. (2014). Evidence for mitochondrial localization of divalent metal transporter 1 (DMT1). *The FASEB Journal*, *28*(5), 2134–2145. https://doi.org/10.1096/fj.13-240564

Xia, Y., Chen, S., Zhu, G., Huang, R., Yin, Y., & Ren, W. (2018). Betaine Inhibits Interleukin-1β Production and Release: Potential Mechanisms. *Frontiers in Immunology*, *9*. https://www.frontiersin.org/articles/10.3389/fimmu.2018.02670

Yi, H., Strauss, J. D., Ke, Z., Alonas, E., Dillard, R. S., Hampton, C. M., Lamb, K. M., Hammonds, J. E., Santangelo, P. J., Spearman, P. W., & Wright, E. R. (2015). Native Immunogold Labeling of Cell Surface Proteins and Viral Glycoproteins for Cryo-Electron Microscopy and Cryo-Electron Tomography Applications. *Journal of Histochemistry & Cytochemistry*, *63*(10), 780–792. https://doi.org/10.1369/0022155415593323

Zeisel, S. H. (2012). A brief history of choline. *Annals of Nutrition & Metabolism*, *61*(3), 254–258. https://doi.org/10.1159/000343120

Zeisel, S. H., Epstein, M. F., & Wurtman, R. J. (1980). Elevated choline concentration in neonatal plasma. *Life Sciences*, *26*(21), 1827–1831. https://doi.org/10.1016/0024-3205(80)90585-8

Zeisel, S. H., Mar, M.-H., Howe, J. C., & Holden, J. M. (2003). Concentrations of choline-containing compounds and betaine in common foods. *The Journal of Nutrition*, *133*(5), 1302–1307. https://doi.org/10.1093/jn/133.5.1302

Zezina, E., Snodgrass, R. G., Schreiber, Y., Zukunft, S., Schürmann, C., Heringdorf, D. M. zu, Geisslinger, G., Fleming, I., Brandes, R. P., Brüne, B., & Namgaladze, D. (2018). Mitochondrial fragmentation in human macrophages attenuates palmitate-induced inflammatory responses. *Biochimica et Biophysica Acta (BBA) - Molecular and Cell Biology of Lipids*, *1863*(4), 433–446. https://doi.org/10.1016/j.bbalip.2018.01.009

Zhang, F., Warskulat, U., Wettstein, M., & Haussinger, D. (1996). Identification of betaine as an osmolyte in rat liver macrophages (Kupffer cells). *Gastroenterology*, *110*(5), 1543–1552. https://doi.org/10.1053/gast.1996.v110.pm8613062

Zhao, G., He, F., Wu, C., Li, P., Li, N., Deng, J., Zhu, G., Ren, W., & Peng, Y. (2018). Betaine in Inflammation: Mechanistic Aspects and Applications. *Frontiers in Immunology*, *9*. https://doi.org/10.3389/fimmu.2018.01070

Zhou, R., Yazdi, A. S., Menu, P., & Tschopp, J. (2011). A role for mitochondria in NLRP3 inflammasome activation. *Nature*, *469*(7329), Article 7329. https://doi.org/10.1038/nature09663

Zhu, X., Song, J., Mar, M.-H., Edwards, L. J., & Zeisel, S. H. (2003). Phosphatidylethanolamine N-methyltransferase (PEMT) knockout mice have hepatic steatosis and abnormal hepatic choline metabolite concentrations despite ingesting a recommended dietary intake of choline. *Biochemical Journal*, *370*(Pt 3), 987–993. https://doi.org/10.1042/BJ20021523

10.0 Contributions of Collaborators

Thank you to Conor O'Dwyer who isolated the hepatocytes in Supplementary Figure 2. The microscopy imaging was performed at the Cell Biology and Image Acquisition Core (RRID: SCR_021845) funded by the University of Ottawa, Ottawa, Natural Sciences and Engineering Research Council of Canada, and the Canada Foundation for Innovation. Metabolites were analysed at the University of Ottawa Metabolomics Core Facility. This facility is supported by the Terry Fox Foundation and Ottawa University. Figure 3, 4 and 12-D were created with BioRender.com.

11.0 Appendix

Supplementary Figure 1: Obtaining a pure mitochondrial fraction in RAW 264.7s. Samples isolated using crude mitochondrial isolation version 2A were diluted in RIPA lysis buffer boiled at 95℃ for 10 min. 8ug of sample was run at 120V for 120 min. CTL2 (65 kDa), β-Actin (45 kDa), TOM20 (20kDa), and Histone3 (15kDa). Whole cell lysate (WCL) was removed prior to mitochondrial isolation.

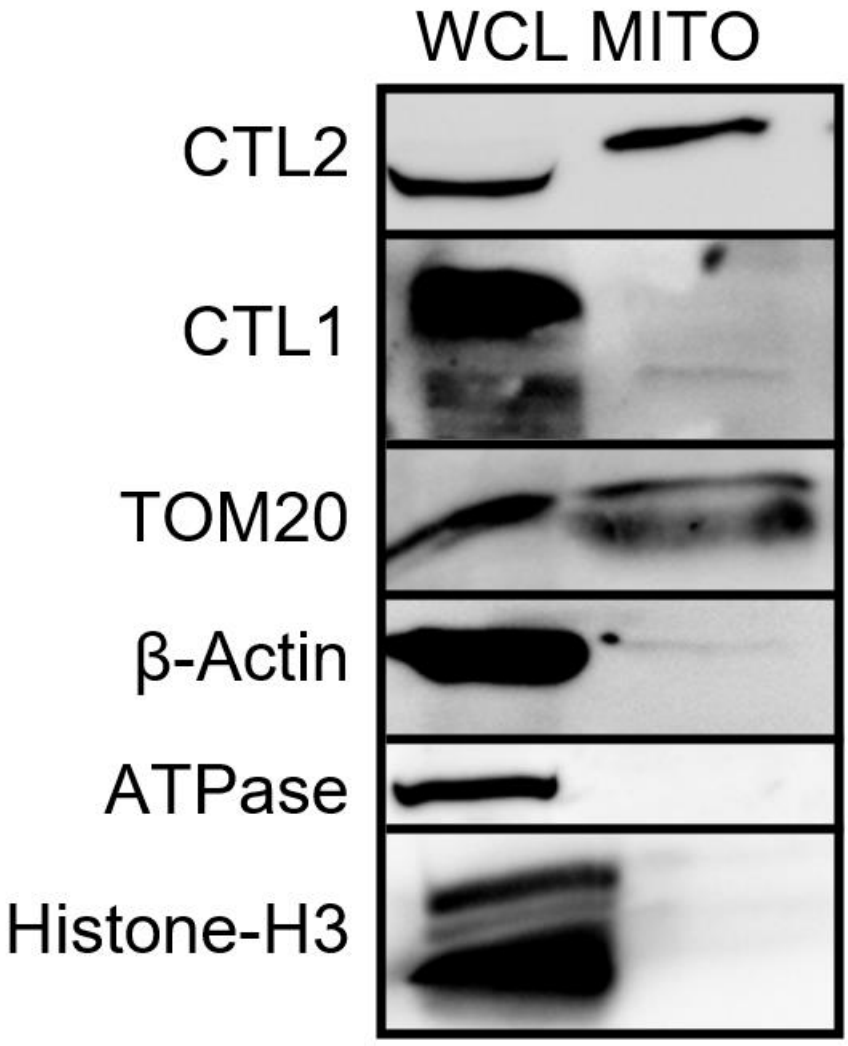
WCL MITO
CTL2
CTL1
TOM20
β-Actin
ATPase
Histone-H3

Supplementary Figure 2: Primary Hepatocytes from WT Mice. Approximately 55,000 hepatocytes were plated on a collagen coated 12 well chamber slide 24 h before fixation. Images were captured on the Z1 epifluorescence widefield microscope at 63X with an LED filter set, then processed through Zen deconvolution. CTL1 (C 21) [top] or CTL2 [bottom] (Red: Alexa fluorophore 647), TOM20 (Green: Alexa fluorophore 488), and DAPI (Blue: nuclear stain). Background stain removal not performed.

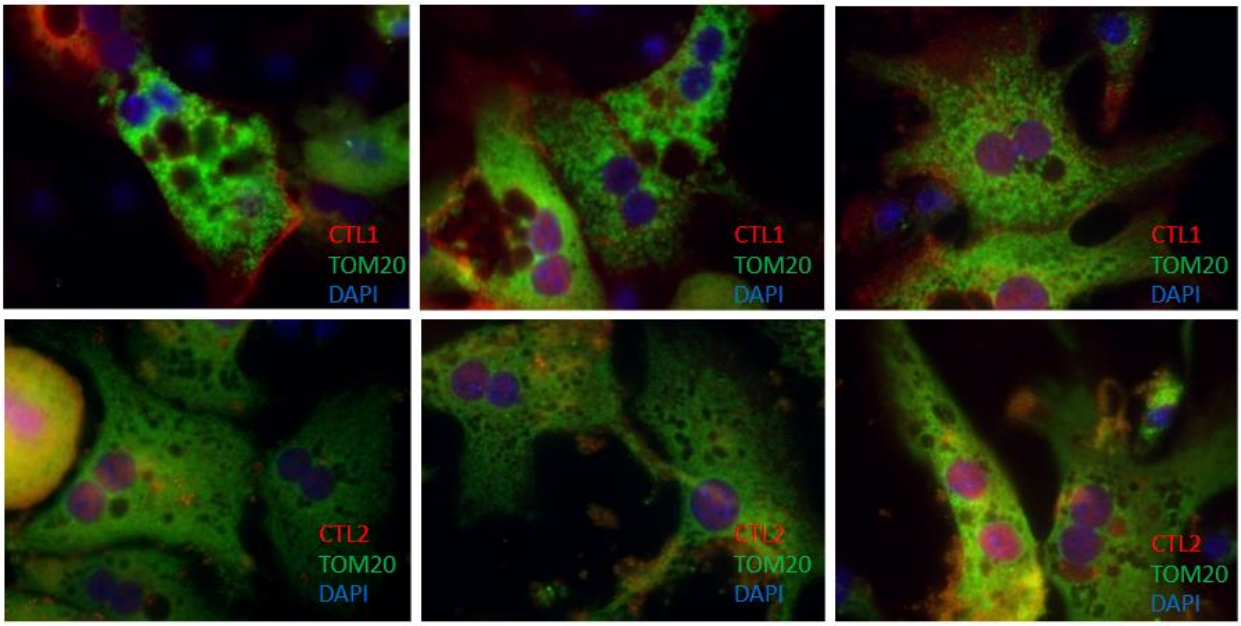
CTL1
TOM20
DAPI
CTL1
TOM20
DAPI
CTL1
TOM20
DAPI
CTL2
TOM20
DAPI
CTL2
TOM20
DAPI
CTL2
TOM20
DAPI

Supplementary Figure 3: Widefield IF images of BMDMs ± LPS processed with deconvolution. 55,000 WT BMDMs were plated on day 6 and received (left) no treatment (NT) or (right) 24 hr LPS stimulation and were fixed at 37℃ with 4% PFA on day 7. Images were captured on a Zeiss Axio-Observer Z1 inverted widefield microscope on a chamber slide (1.5mm coverslip) with the 63X objective and LED filter set, then processed through Zen fast iterative deconvolution. CTL2 (Green: Oregon Green 488), MT (Red: MitoTracker™ CMXRos), and DAPI (Blue: nuclear stain).

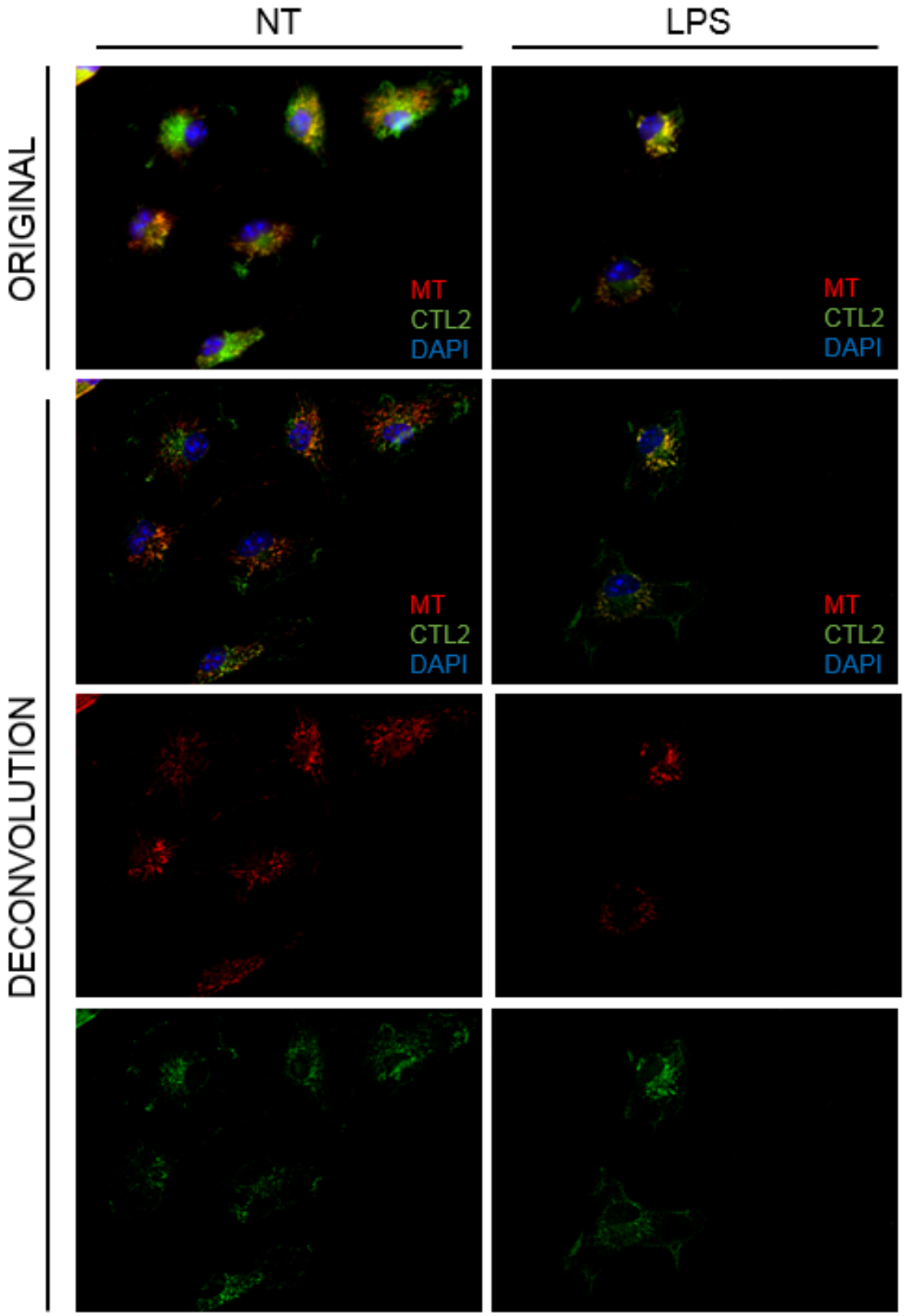
NT
LPS
ORIGINAL
DECONVOLUTION
MT
CTL2
DAPI
MT
CTL2
DAPI
MT
CTL2
DAPI
MT
CTL2
DAPI

Supplementary Figure 4: Background stain removal. Individual stains of CTL1, CTL2, and MT taken with background removal applied to Figures 9-11. Each well was stained with indicated stains only.

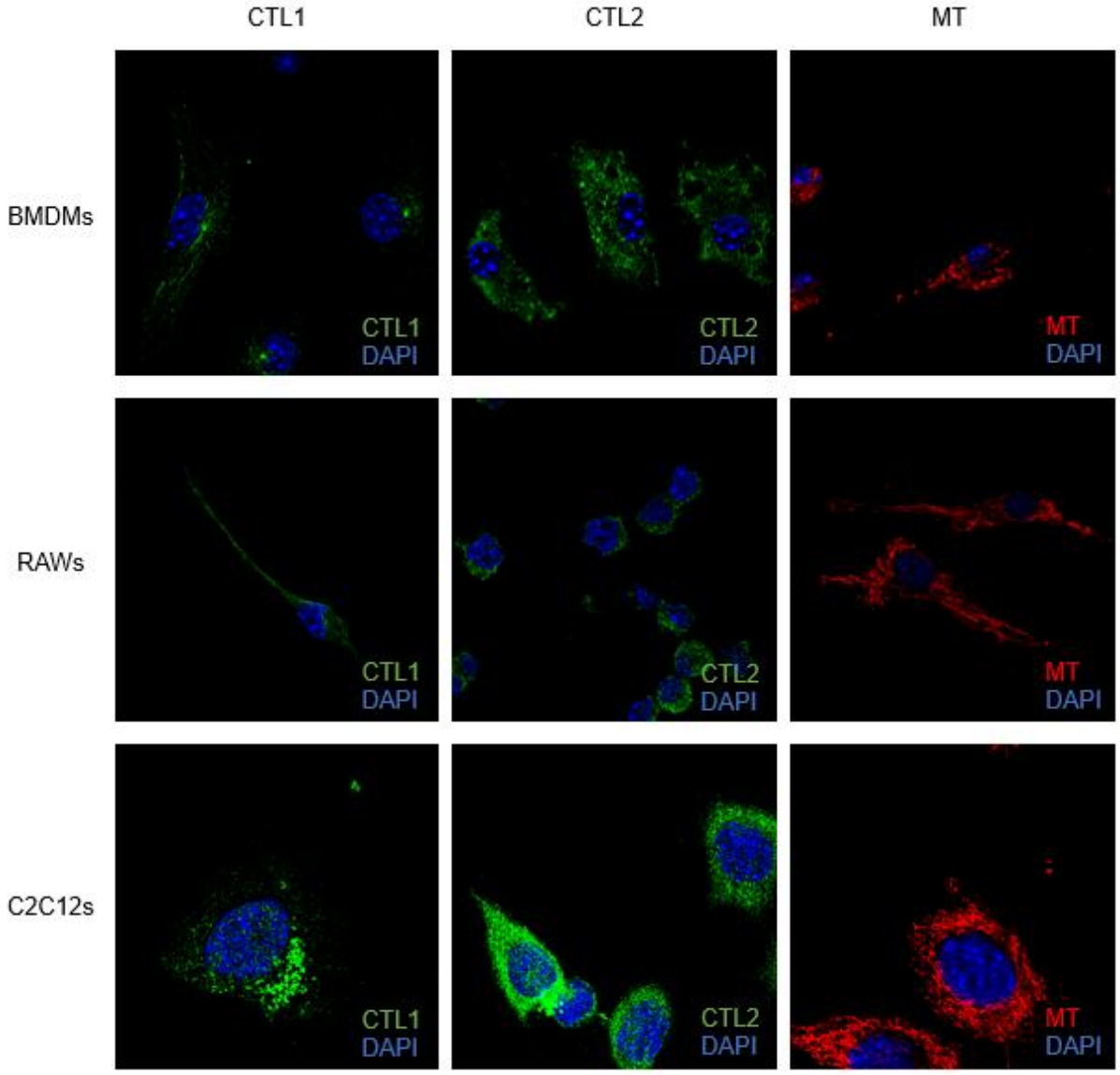

Supplementary Figure 5: C2C12 Voxel Visualization. (A) Imaris 3D rendering performed on C2C12s. (B) Quantification displayed as ratio between volume of overlap between CTL1-MT to volume of mitochondria.

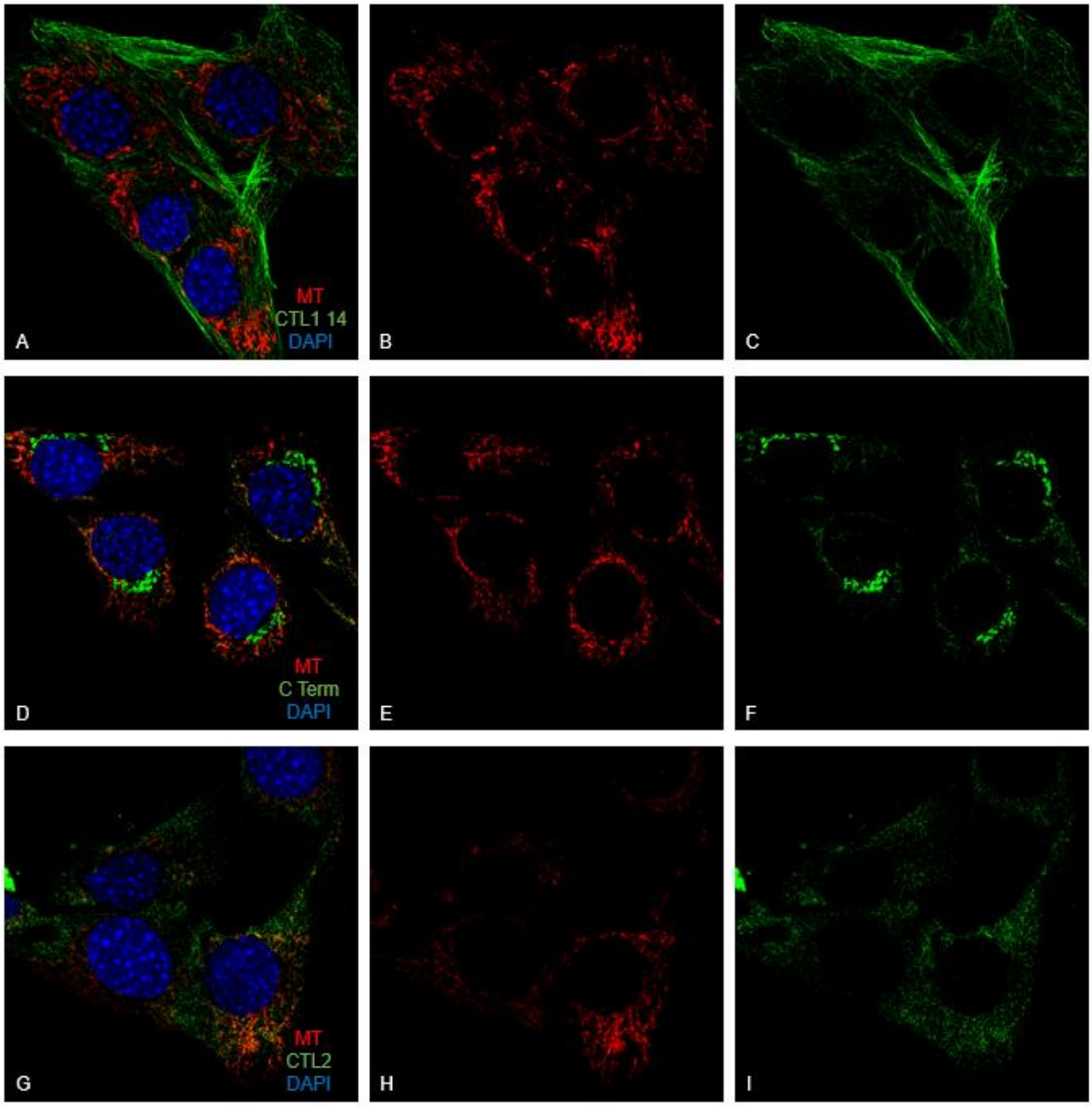
MT
CTL1 14
DAPI
A
B
C
MT
C Term
DAPI
D
E
F
MT
CTL2
DAPI
G
H
I

Supplementary Figure 6: Detecting co-localization of C2C12 mitochondria and CTL proteins. 10,000 C2C12s P.14 allowed to adhere for 24 h were fixed at 37℃ with 4% PFA. Images were captured on a Zeiss Axio-ObserverZ1-LSM 880-AiryScan confocal microscope on a chamber slide (1.5mm coverslip) 63x objective, using the AiryScan detector. CTL1/2 (Green: Oregon Green 488), MT (Red: MitoTracker™ CMXRos), and DAPI (Blue: nuclear stain). Red-green overlap shown in yellow. CTL1 14 (C 14).

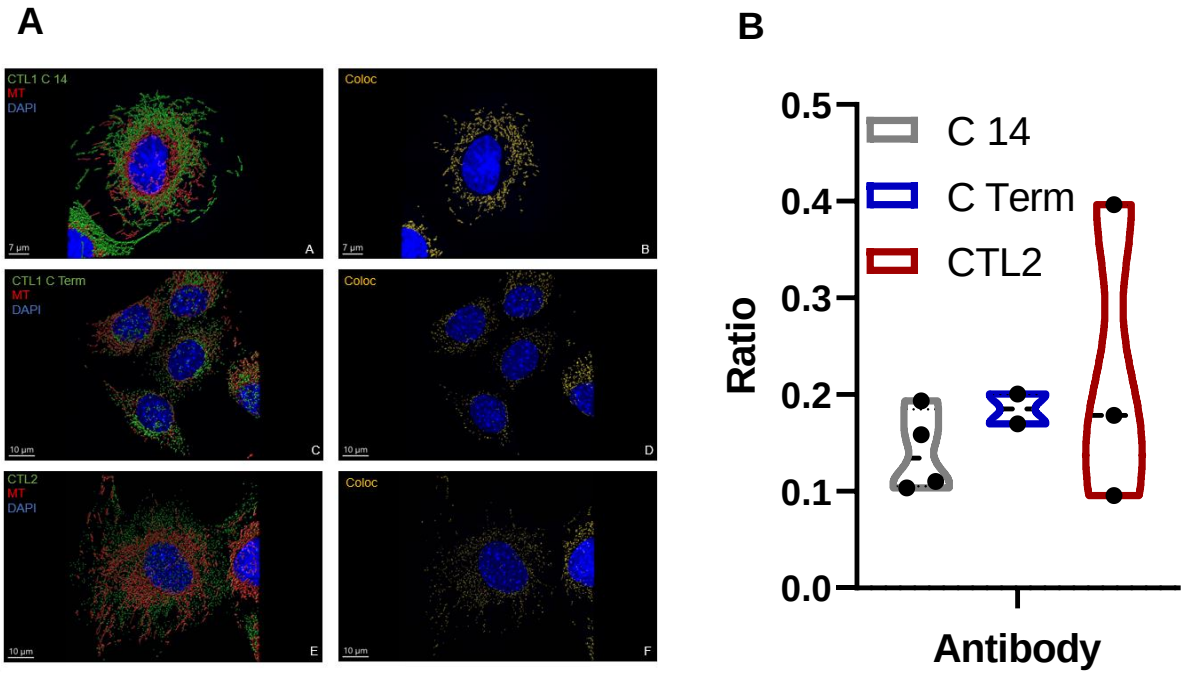
A
CTL1 C 14
MT
DAPI
7 µm
A
Coloc
7 µm
B
CTL1 C Term
MT
DAPI
10 µm
C
Coloc
10 µm
D
CTL2
MT
DAPI
10 µm
E
Coloc
10 µm
F
B
0.5
0.4
0.3
0.2
0.1
0.0
Ratio
C 14
C Term
CTL2
Antibody

Supplementary Table 1: Individual values used to report the ratio of colocalization in BMDMs. Various replicates were taken from different cells of the same well for an N=1.

Volume of CTL Co-Loc	Volume of Mito	Ratio
CTL1 NT		
15.78	168.94	0.0934
13.15	68.44	0.1921
4.30	52.51	0.0819
16.67	109.74	0.1519
10.58	75.93	0.1393
7.67	125.11	0.0613
CTL1 LPS		
13.34	92.76	0.1438
16.80	94.92	0.1767
28.60	302.34	0.0946
22.67	108.04	0.2098
38.67	243.61	0.1587
19.78	145.66	0.1358
16.51	174.81	0.0944
15.24	189.12	0.0806
18.91	120.34	0.1571
39.31	292.09	0.1346
40.31	235.00	0.1718
27.76	278.11	0.0998
CTL2 NT		
15.55	49.03	0.3172
35.34	183.03	0.1931
7.16	174.45	0.0410
24.19	169.91	0.1424
8.71	135.71	0.0642
3.91	70.13	0.0558
CTL2 LPS		
37.49	96.09	0.3902
74.63	207.93	0.3589
76.23	236.28	0.3226
93.33	237.08	0.3937
67.45	166.28	0.4056
72.73	273.58	0.2658
73.17	259.78	0.2816
80.31	151.90	0.5287
33.31	150.39	0.2215

Supplementary Table 2: Individual values used to report the ratio of colocalization in RAW47s. Various replicates were taken from different cells of the same well for an N=1.

Volume of CTL Co-Loc	Volume of Mito	Ratio
CTL1 NT		
28.24	64.11	0.4405
50.85	112.92	0.4503
57.52	150.03	0.3834
104.51	254.10	0.4113
CTL1 LPS		
83.28	300.63	0.2770
65.63	233.8	0.2807
69.20	225.81	0.3065
102.59	313.01	0.3278
94.98	289.76	0.3278
CTL2 NT		
26.26	93.53	0.2808
81.99	245.49	0.3310
59.57	119.93	0.4967
CTL2 LPS		
107.64	236.92	0.4543
103.48	225.14	0.4596
96.66	281.18	0.3438
56.91	178.04	0.3196
63.60	141.08	0.4508

Supplementary Table 3: Individual values used to report the ratio of colocalization in C2C12s. Various replicates were taken from different cells of the same well for an N=1.

Volume of CTL Co-Loc	Volume of Mito	Ratio
CTL1 C14		
35.36	341.12	0.1037
28.74	181.14	0.1587
27.28	141.00	0.1935
61.11	554.73	0.1102
CTL1 C Term		
48.93	244.07	0.2005
45.32	266.75	0.1699
CTL2		
280.25	706.61	0.3966
44.86	469.91	0.0955
105.58	590.70	0.1787